The relation between degree-2160 spectral models of Earth's gravitational and topographic potential - a guide on global correlation measures and their dependency on approximation effects

Christian Hirt[1,2]*, Moritz Rexer[1,2], Sten Claessens[3], and Reiner Rummel[1]

[1]Institute for Astronomical and Physical Geodesy,
Technische Universität München, Arcisstr 21, 80333 München, Germany

[2]Institute for Advanced Study, Technische Universität München, Germany

[3]Western Australian Geodesy Group & The Institute for Geoscience Research,
Curtin University, GPO Box U1987, Perth, WA 6845, Australia

* Corresponding author, c.hirt@tum.de

Abstract

Comparisons between high-degree models of the Earth's topographic and gravitational potential may give insight into the quality and resolution of the source data sets, provide feedback on the modelling techniques and help to better understand the gravity field composition. Degree correlations (cross-correlation coefficients) or reduction rates (quantifying the amount of topographic signal contained in the gravitational potential) are indicators used in a number of contemporary studies. However, depending on the modelling techniques and underlying levels of approximation, the correlation at high degrees may vary significantly, as do the conclusions drawn.

The present paper addresses this problem by attempting to provide a guide on global correlation measures with particular emphasis on approximation effects and variants of topographic potential modelling. We investigate and discuss the impact of different effects (e.g., truncation of series expansions of the topographic potential, mass-compression, ellipsoidal vs. spherical approximation, ellipsoidal harmonic coefficient (EHC) vs. spherical harmonic coefficient (SHC) representation) on correlation measures. Our study demonstrates that the correlation coefficients are realistic only when the model's harmonic coefficients of a given degree are largely independent of the coefficients of other degrees, permitting degree-wise evaluations. This is the case, e.g., when both models are represented in terms of SHCs and spherical approximation (i.e., spherical arrangement of field-generating masses). Alternatively, a representation in ellipsoidal harmonics can be combined with ellipsoidal approximation. The usual ellipsoidal approximation level (i.e., ellipsoidal mass arrangement) is shown to bias correlation coefficients when SHCs are used. Importantly, gravity models from the International Centre for Global Earth Models (ICGEM) are inherently based on this approximation level. A transformation is presented that enables a transformation of ICGEM geopotential models from ellipsoidal to spherical approximation. The transformation is applied to generate a spherical transform of EGM2008 (sphEGM2008) that can meaningfully be correlated degree-wise with the topographic potential.

We exploit this new technique and compare a number of models of topographic potential constituents (e.g., potential implied by land topography, ocean water masses) based on the Earth2014 global relief model and a mass-layer forward modelling technique with sphEGM2008. Different to previous findings, our results show very significant short-scale correlation between Earth's gravitational potential and the potential generated by Earth's land topography (correlation +0.92, and 60 % of EGM2008 signals are delivered through the forward modelling). Our tests reveal that the potential generated by Earth's oceans water masses is largely unrelated to the geopotential at short scales, suggesting that altimetry-derived gravity and/or bathymetric data sets are significantly underpowered at 5 arc-min scales. We further decompose the topographic potential into the Bouguer shell and terrain correction and show that they are responsible for about 20% and 25% of EGM2008 short-scale signals, respectively. As a general conclusion, the paper shows the importance of using compatible models in topographic/gravitational potential comparisons and recommends the use of SHCs together with spherical approximation or EHCs with ellipsoidal approximation in order to avoid biases in the correlation measures.

Key words: Correlation coefficient, degree correlation, reduction rate, gravitational potential, topographic potential, gravity forward modelling

1 Introduction

In global gravity field studies, spectral models of the observed gravitational potential and the topography or topographic potential are often compared with each other. The correlation, computed from the model coefficients as a function of the harmonic degree, serves as an important measure to characterise the mutual relationship between observed and topographic gravitation at different spatial scales (e.g., Lambeck 1976, Phillips and Lambeck 1980, Rapp 1982, Kaula 1992, Wieczorek 2015).

The correlation between gravitational and topographic potentials has been used to investigate the gravity field characteristics of planetary bodies such as the Moon (e.g., Zuber et al. 2013, Lemoine et al. 2014), Venus (Ananda et al. 1980, Konopliv et al. 1999), Mars (McGovern et al. 2002, Konopliv 2016) and Earth (e.g., Lambeck 1976, Novak 2010, Hirt et al. 2012, Tsoulis and Patlakis 2013, Wieczorek 2015, Rexer et al. 2016), which is the focus of this study.

At lower harmonic degrees, correlations between observed and topographic potential may give insight into the state of isostatic compensation of the topography of a planetary body (e.g., Lambeck 1976, McGovern et al. 2002). At higher harmonic degrees, correlations can be useful to assess the quality of the models involved (e.g., Mazarico et al. 2010). This is because the near-surface topographic masses are the main contributor to short-scale gravitational field variations (e.g., Tziavos and Sideris 2013). Usually, detailed knowledge of the topography is utilised to assess the (short-scale) quality of gravity field models from space observations of, e.g., the Earth (Hirt et al. 2012, Hirt et al. 2015), but also other planetary bodies such as the Moon (Mazarico et al. 2010, Lemoine et al. 2014). However, the approach can be reversed by deploying a reliable gravity model of sufficient resolution to assess the quality of a topography or crustal mass model (Hirt 2014, Tenzer et al. 2015).

One may argue that correlation coefficients are straightforward to use in studies aiming to investigate the relationship between models of Earth's gravity potential and topography. Indeed, this is the case for low and medium-resolution spectral models, say up to harmonic degree 180 or even 360 and there are no significant differences for different modelling approaches (cf. Fig. 1). However, the situation is entirely different in the presence of modern Earth gravity models such as EGM2008 (Pavlis et al. 2012) or EIGEN-6C4 (Förste et al. 2015), both of which offer a resolution of 5 arc-min or harmonic degree ~2,160.
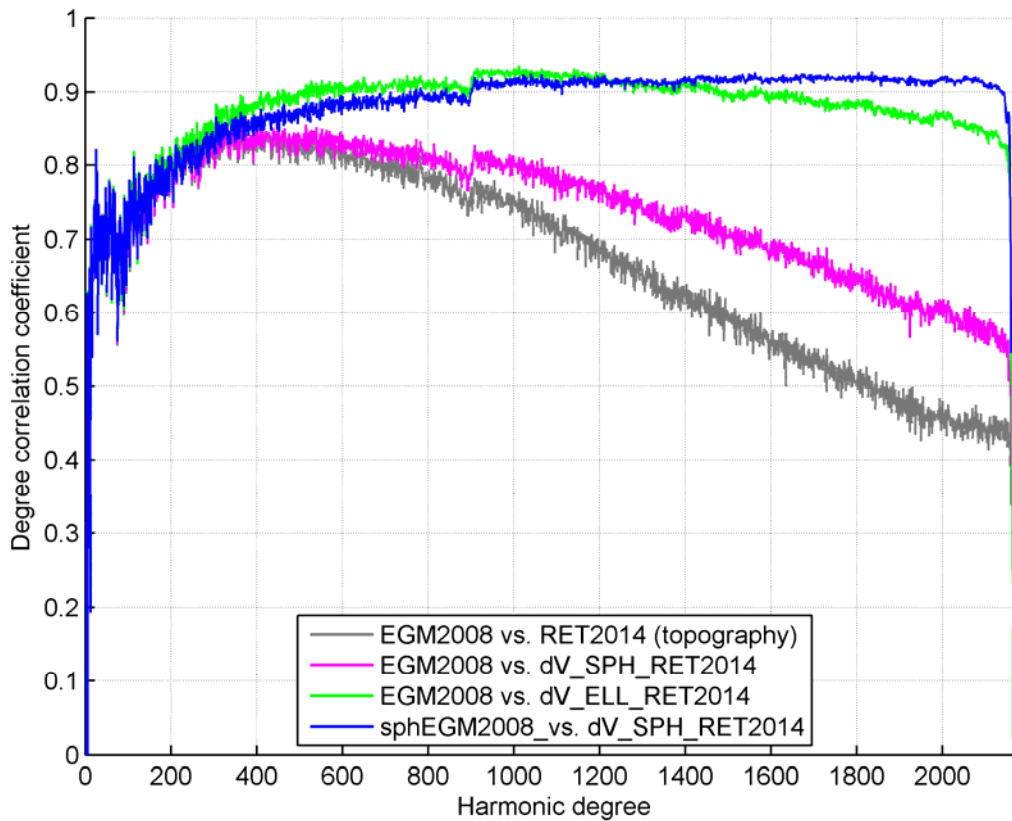
Fig. 1. Correlation coefficients between EGM2008 and the topography (grey), EGM2008 and the topographic potential in spherical approximation (magenta), EGM2008 and the topographic potential model in ellipsoidal approximation (green) and a new spherical transform of EGM2008 (this work, Sect. 3.2) vs. the topographic potential in spherical approximation (blue). The figure shows a broad spectrum of CC behaviour depending on the underlying approximation or modelling approach.

As our starting point, Fig. 1 shows degree correlation coefficients computed between four different model pairs representing Earth's gravitational and topographic potential (all of which are further explained in this paper). In Fig. 1, both the gravitational and the topographic potential are based on different levels of approximation (spherical and ellipsoidal, see explanations in Sect. 2.3), and one topographic potential model variant deliberately assumes linearity between topographic heights and implied topographic potential, used as approximation in some of the early literature on correlation analyses.

Figure 1 reveals a very different behaviour of the correlation curves for the medium and high-frequency spectrum, with the correlation varying considerably between +0.45 (moderate correlation) and +0.92 (significant correlation) at harmonic degree 2000, and only one model pair reaching maximum correlation near the full resolution of the gravity model. Thus, with degree-2160 models, a number of effects come into play that have strong impact on the correlation coefficients at medium and high harmonic degrees.

Some of the approximations behind the correlation curves shown in Fig. 1 were utilised in the contemporary literature dealing with the relationship between Earth's topographic and gravitational potential (e.g., Novak 2010, Hirt et al. 2012, Claessens and Hirt 2013, Wieczorek 2015, Grombein et al. 2016, Rexer et al. 2016). Our Fig. 1 raises questions as to why the correlation curves are so different and which offers most reliable information on the correlation between Earth's gravity and topography, globally and at short spatial scales.

In light of the different results found in recent studies, the present paper attempts to provide a guide on global correlation measures between high-degree Earth gravitational and topographic potential models. This includes a compilation, comparison and discussion of (a) approximation effects and of (b) different variants of topographic potential modelling on the correlation values.

The paper is organised as follows. Section 2 compiles some background information and concepts relevant to this paper. This includes general remarks on the differences between the topographic and gravitational potential, a brief review of spherical and ellipsoidal harmonic field representations, and a definition of the spherical and ellipsoidal approximation level. Section 3 presents the methods used, including a description of the spectral-domain gravity forward modelling, a new transformation for gravitational models from ellipsoidal to spherical approximation and the definition of correlation measures (degree correlation coefficients and degree reduction rates) applied. Section 4 then provides an overview of the data sets and models utilised in our study. Section 5 as the main part of this paper compiles and investigates a number of different effects (e.g., truncation of series expansions of the topographic potential, mass-compression, ellipsoidal vs. spherical approximation, ellipsoidal vs. spherical harmonic representations) on the correlation coefficients and correlates different constituents of the topographic potential (e.g., land topography, ocean water, ice sheets) with Earth's gravitational potential. Section 6 discusses the results – also in the context of the literature, and Section 7 summarises the main conclusions of the paper.

We acknowledge that correlations can be evaluated in both the spatial or spectral domain, and on a global scale or with localisation over a specific area (McGovern et al. 2002, Wieczorek and Simons 2005, Hirt et al. 2015, Simons et al. 1997). The present study focusses on (global) correlations computed in the spectral domain in the context of high-degree Earth gravity field modelling. However, some insights obtained in our study might be useful for future correlation studies with localisation in the spectral or spatial domain.

Abbreviations frequently used in this paper:

SHC – spherical harmonic coefficient

EHC – ellipsoidal harmonic coefficient

SA – spherical approximation

EA – ellipsoidal approximation

STP – spherical topographic potential

ETP – ellipsoidal topographic potential

GGM – Global Gravity Model

CC – correlation coefficient

RR – reduction rate

2. Background

For a better understanding of some differences among topographic and gravitational potential models, and the context of this work, some modelling concepts are explained here.

2.1 Gravitational vs. topographic potential

The gravitational potential, as can be observed (indirectly) at or above the Earth's surface, is generated by all masses within the Earth's body, a consequence of Newton's universal law of gravitation (e.g., Torge and Müller 2012). Opposed to this, the topographic potential – as commonly used in other studies, e.g., Novak (2010), Wieczorek (2015), Grombein et al. (2016) – denotes the gravitational potential generated by those masses near the Earth's surface with reasonably well-known geometry and mass-density. The near-surface masses usually considered in topographic potential modelling naturally encompass the topographic masses over land areas, but also the masses of ocean and lake water and ice-sheets. To obtain the topographic potential model from the mass distribution, some forward gravity modelling technique is needed and applied (e.g., Hirt and Kuhn 2014).

Leaving modelling and data errors aside, the key difference between the (observed) gravitational and (forward-modelled) topographic potential is the gravitational effect of all unknown masses contained in the observed potential. These are, for instance, mass-anomalies within the (often assumed as homogenous) topographic masses or unmodelled masses in the interior of the Earth. The gravitational effect of the latter, however, attenuates with increasing spatial resolution (or harmonic degree) on the one hand, and increasing depth on the other hand. Particularly at shorter spatial scales, the topographic masses are therefore the main contributor to the gravitational potential (e.g., Forsberg and Tscherning, 1981; Tziavos and Sideris, 2013) and a high correlation can be expected between gravity and topography with increasing harmonic degree. This, however, necessitates the spherical harmonic topographic and gravitational potential models to be as compatible as possible. The compatibility between the models involved is the key aspect of this paper.

2.2. Ellipsoidal vs. spherical harmonics

This study is concerned with the correlation between spectral models of the Earth's gravitational and topographical potential, as can be obtained, e.g., via the International Association of Geodesy (IAG)'s International Centre for Global Earth Models (ICGEM, http://icgem.gfz-potsdam.de/ICGEM/). Generally, gravitational or topographical potential models can be represented in terms of spherical or ellipsoidal harmonic series expansions. In most practical uses, the potential model is represented in terms of spherical harmonic coefficients (SHCs), which can be more easily evaluated than series using ellipsoidal harmonic coefficients (EHCs), e.g., in terms of various functionals of the potential. On the other hand, ellipsoidal harmonic series offer the advantage of potentially better convergence behaviour in the vicinity of the masses (e.g., Holmes and Pavlis 2007, Lowes and Winch 2012, Hu and Jekeli 2015). Thus far, all potential models distributed via ICGEM are represented in terms of SHCs.

2.2.1 Spherical harmonics

At a point P (φ, λ, r) exterior to the mass distribution, where φ denotes the geocentric latitude, λ the longitude and r the geocentric radius of evaluation, the potential V is obtained via (Sanso and Sideris, 2013):

$$V(\varphi, \lambda, r) = \frac{GM}{R} \sum_{n=2}^{N_{max}} \left(\frac{R}{r}\right)^{n+1} \sum_{m=-n}^{n} \bar{V}_{nm} \bar{Y}_{nm}(\varphi, \lambda)$$

(1)

where *GM* and *R* are the model-specific constants (*GM*: product of universal gravitational constant and Earth's mass, *R*: model reference radius), N_{max} denotes the maximum degree of evaluation and $\bar{Y}_{nm}(\varphi, \lambda)$ are the base functions (fully-normalised associated Legendre Functions of degree n and order m)

$$\bar{Y}_{nm}(\varphi, \lambda) = \bar{P}_{n|m|}(\sin\varphi)\begin{cases}\cos m\lambda & \text{for } m \geq 0 \\ \sin|m|\lambda & \text{for } m < 0\end{cases} \tag{2}$$

and $\bar{V}_{nm}$ is the short-hand notation for the fully normalised SHCs $(\bar{C}_{nm}, \bar{S}_{nm})$ of degree n and order m

$$\bar{V}_{nm} = \begin{cases}\bar{C}_{nm} \text{ for } m \geq 0 \\ \bar{S}_{n|m|} \text{ for } m < 0\end{cases} \tag{3}$$

2.2.2 Ellipsoidal harmonics (EHCs)

Alternatively and equivalently, the gravitational or topographic potential can be expressed in terms of (oblate) spheroidal harmonic coefficients, which are sometimes in the literature and in this paper denoted as ellipsoidal harmonic coefficients (EHCs), also see Hobson (1965), Jekeli (1988), and Pavlis et al. (2012). Following Hu and Jekeli (2015), the external potential is obtained as series expansion via

$$V(\beta, \lambda, u) = GM \sum_{n=2}^{N'_{max}} \sum_{m=-n}^{n} \frac{Q_{nm}(i\frac{u}{E})}{Q_{nm}(i\frac{b}{E})} \bar{V}'_{nm} \bar{Y}_{nm}(\beta, \lambda) \tag{4}$$

where N'_{max} is the maximum ellipsoidal harmonic degree, the coordinate triplet (β, λ, u) denote the reduced latitude, longitude and semi-minor axis associated with the computation point, b is the semi-minor axis of the bounding spheroid of focal length E, $i = \sqrt{-1}$, and Q_{nm} are the associated Legendre functions of the second kind of degree n and order m, and $\bar{V}'_{nm}$ are the EHCs

$$\bar{V}'_{nm} = \begin{cases}\bar{C}'_{nm} \text{ for } m \geq 0 \\ \bar{S}'_{n|m|} \text{ for } m < 0\end{cases} \tag{5}$$

The spherical harmonic expansion (Eq. 1) can be considered a special case of the ellipsoidal harmonic expansion (Eq. 4), when the semi-major and semi-minor axes of the reference ellipsoid are identical (e.g., Heiskanen and Moritz 1967, Claessens 2016). We acknowledge that the use of the term "ellipsoidal harmonics" is somewhat ambiguous, as it is used to denote a solution to Laplace's equation in ellipsoidal coordinates (e.g., Hu and Jekeli 2015) on the one hand, and for oblate spheroidal harmonics (Pavlis et al. 2012) on the other hand; also see Lowes and Winch (2012, p 506-507).

High-resolution potential models are sometimes developed in terms of EHCs (for a discussion of the advantages, see, e.g., Holmes and Pavlis 2007), but eventually made available to the user community in terms of SHCs, which are more convenient to work with in practice. EHCs are included in the present study because they can be a means to compute realistic correlation coefficients between topographic and gravitational potential models at short scales (cf. Rexer et al. 2016).

2.2.3 SHC – EHC transformation

SHCs can be transformed to EHCs and vice versa using the exact transformation by Jekeli (1988). In brief, the (forward) conversion from SHCs $\bar{V}_{nm}$ to EHCs $\bar{V}'_{nm}$ reads (after Jekeli 1988, p111; Lowes and Winch 2012, p500; Sebera et al. 2012, Claessens 2016)

$$\bar{V}'_{nm} = \bar{F}_{nm}(E, b, R) \sum_{l=0}^{w} \delta_{nml} \, \bar{V}_{n-2l,m} \tag{6}$$

$$w = \mathrm{int}\left(\frac{n - |m|}{2}\right) \tag{7}$$

where $\bar{F}_{nm}$ are scaling functions (aka renormalised associated Legendre functions of the second kind) that depend on the reference ellipsoid parameters (E, b) and the radius of the reference sphere R, δ_{nml} are the weights (see Jekeli 1988, p111 for full expressions of the scaling functions and weights). The (backward) transformation can be used to obtain SHCs $\bar{V}_{nm}$ as a function of EHCs $\bar{V}'_{nm}$:

$$\bar{V}_{nm} = \sum_{l=0}^{w} \frac{\Delta_{nml}}{\bar{F}_{nm}(E, b, R)} \, \bar{V}'_{n-2l,m} \tag{8}$$

where Δ_{nml} are weights computed with Jekeli (1988, Eq. 35). Eq. (8) was applied by Pavlis et al. (2012) to obtain the SHCs of EGM2008 from the corresponding EHC model representation. Both in the forward and backward transformation, "*the transformation is entirely within coefficients of a given order m*" (Lowes and Winch 2012, p501). The transformed coefficients of degree n depend on input coefficients within a "window" from degree $n - w$ to $n + w$. This windowing effect introduces functional correlations between brackets of coefficients, which has important consequences on the correlation between gravitational and topographic potential models, as will be shown in Sect. 5.

2.3 Ellipsoidal vs. spherical approximation

Of central importance for this study is the arrangement of the field-generating masses. If the topographic masses are arranged relative to a mass-sphere, the resulting model is said to be based on "spherical approximation", while "ellipsoidal approximation" denotes the mass arrangement relative to a mass-ellipsoid (cf. Claessens and Hirt 2013, Rexer and Hirt 2015).

Gravitational potential models – as available via ICGEM's table of models – rely on observed functionals of the gravitational field, which are generated by all of Earth's masses. Because the shape of Earth is much closer to an ellipsoid of revolution than a sphere, the arrangement of field-generating masses is in good approximation ellipsoidal. As a result, ICGEM's gravitational potential models (available via http://icgem.gfz-potsdam.de/ICGEM/, Table of Models) can generally be considered to inherently rely on ellipsoidal approximation.

Opposed to this, in topographic potential modelling there are no field observations involved that would implicitly determine the approximation level of the model. Instead, the modeller can choose to either arrange the masses in spherical or ellipsoidal approximation (also see Sect. 3.1).

- In spherical approximation, the topography is "mapped" onto the surface of a sphere (e.g., Rummel et al. 1988, Novak 2010, Balmino et al. 2012, Hirt and Kuhn 2014). The resulting spherically approximated model of the topographic potential is also known as STP (spherical topographic potential). In other words, in the STP, the topography is assumed to reside above a reference sphere (i.e. the orthometric or ellipsoidal heights of topography are taken as if measured above a reference sphere). This can be interpreted as a 'morphing' of the Earth's shape to a more spherical shape, ignoring its considerable flattening.

- In ellipsoidal approximation, the topography is modelled relative to a reference ellipsoid (Wang and Yang 2013, Claessens and Hirt 2013, Grombein et al. 2016, Rexer et al. 2016). The

topography can be expressed in terms of ellipsoidal heights (e.g., obtained by referring an Earth shape model to a reference ellipsoid), such that mapping or morphing can be avoided. Gravity forward modelling based on ellipsoidal approximation yields models of the so-called ellipsoidal topographic potential (ETP, Claessens and Hirt 2013).

A detailed qualitative and quantitative investigation of the mapping and involved approximation differences in STP and ETP models can be found in Rexer et al. (2016).

Crucially, approximation levels (spherical vs. ellipsoidal) and type of harmonic expansion (spherical vs. ellipsoidal) are not the same and must be clearly distinguished. In summary, "approximation level" specifies the spatial arrangement of the field-generating masses, with spherical approximation denoting a mass-arrangement relative to a sphere and ellipsoidal approximation relative to an ellipsoid. The "type of harmonic expansion" (Sect. 2.2) specifies whether spherical harmonic or ellipsoidal harmonic series expansions are used as spectral representation. The differences are summarized in Table 1, along with model examples.

The gravity field functionals are invariant w.r.t. the type of harmonic expansion (within the convergence regions, cf. Jekeli and Hu 2015), but show minor dependence on the approximation level (see e.g. Rexer et al. 2016). However, the spectra and correlation measures may depend on the type of harmonic expansion and approximation level, as shown in Sect. 4 and 5.

Tab. 1 Summary of spherical and ellipsoidal harmonic coefficients and approximation levels and examples

Property	Spherical	Ellipsoidal
Harmonic coefficients	Sect. 2.2.1 and Eq. 1 ICGEM's "Table of models" and ICGEM's "Models related to topography "	Sect. 2.2.2 and Eq. 4
Approximation level of the topographic potential	Sect. 3.1 and Eq. (11) e.g., dV_SPH_Earth2014	Sect. 3.1 and Eq. (9) ICGEM's "Models related to topography ", e.g., dV_ELL_Earth2014
Approximation level of the gravitational potential	Sect. 3.2 and Eq. (13) e.g., sphEGM2008	ICGEM's "Table of models", e.g., EGM2008

The model collection of IAG's International Centre for Global Earth Models (ICGEM) is available via http://icgem.gfz-potsdam.de/ICGEM/

3. Methods

This section gives a brief overview of the spectral-domain gravity forward modelling approach used to generate most of the topographic potential models used in this study (Sect. 3.1). We also describe an approach to transform (observation-based) gravitational potential models from ellipsoidal to spherical approximation (Sect. 3.2) that will be shown to be helpful for obtaining realistic correlation coefficients. The section concludes with a definition of correlation measures used to quantify the relation between gravitational and topographic potential models (Sect 3.3).

3.1 Gravity forward modelling

The spectral-domain gravity forward modelling technique derived in Rexer et al. (2016) models the topographic potential based on superposition of an arbitrary number of mass-layers of constant density (e.g., topography, water masses, ice masses). The approach is capable of delivering the topographic potential in either spherical or ellipsoidal approximation. Next, we describe the mathematical formalism of the layer-based spectral-domain forward modelling in order to illustrate the origin of some approximation effects on correlation measures (Sect. 5). These include the choice of the approximation level (spherical vs. ellipsoidal approximation) on the one hand and the truncation effect (approximation of the topographic potential as series expansion of a limited number of integer powers of the topography) on the other hand.

The SHCs of the ellipsoidal topographic potential that is generated by the masses of volumetric layers Ω_ω of constant mass-density - with their boundaries defined with respect to a reference ellipsoid – are obtained through (cf. Rexer et al. 2016)

$$
\bar{V}_{nm}^{ETP} = \frac{3}{\bar{\rho}(2n+1)(n+3)} \left(\frac{b}{R}\right)^{n+3} \sum_{k=1}^{k_{max}} \binom{n+3}{k} \sum_{j=0}^{j_{max}} (-1)^j \binom{-\frac{n+3}{2}}{j} e^{2j} \times
$$
$$
\sum_{i=-j}^{j} \bar{K}_{nm}^{2i,2j} \sum_{\omega=1}^{\omega_{max}} \overline{HDF}_{klm}^{(ETP,\,\Omega_\omega)}
\tag{9}
$$

where $\bar{\rho}$ is the mean density of Earth, b the semi-minor axis of the reference ellipsoid, R the reference radius for the SHCs, k_{max} is the maximum order of the first binominal series expansion, j_{max} is the maximum order of the second binominal series expansion, e^2 is the squared first eccentricity of the reference ellipsoid, $\bar{K}_{nm}^{2i,2j}$ are the sinusoidal Legendre weight functions (Claessens 2006), Ω_ω denotes the volumetric-mass layer, and ω_{max} the maximum number of layers modelled and $l = n + 2i$. From Rexer et al. (2016), values of $k_{max} = 12$ and j_{max} = 30 have been found to ensure convergence for degree-2190 expansions.

The fully-normalised surface spherical harmonic coefficients $\overline{HDF}_{klm}^{(ETP,\,\Omega_\omega)}$ of the height density-function of the mass layer Ω_ω must be determined separately for every mass layer according to

$$
\overline{HDF}_{klm}^{(ETP,\,\Omega_\omega)} = \frac{1}{4\pi} \int_{\lambda=0}^{2\pi} \int_{\varphi=0}^{\pi} \rho^{(\Omega_\omega)} \left(\left(\frac{d_{UB}^{(\Omega_\omega)}}{r_e}\right)^k - \left(\frac{d_{LB}^{(\Omega_\omega)}}{r_e}\right)^k \right) \bar{Y}_{lm}(\varphi,\lambda) \, \cos\varphi \, d\varphi d\lambda
\tag{10}
$$

by means of multiple spherical harmonic analyses, e.g. by quadrature (Colombo 1981, Rexer and Hirt, 2015). In Eq. (10), $\rho^{(\Omega_\omega)}$ is the (constant) mass-density of the respective layer Ω_ω, r_e the ellipsoidal radius, and $d_{UB}^{(\Omega_\omega)}, d_{LB}^{(\Omega_\omega)}$ denote the approximated ellipsoidal heights of the respective layer's upper bound (UB) and lower bound (LB).

Quite similar to the "windowing" that occurs in Jekeli's transform (EHC to SHC, Sect. 2.2.3), ETP models also have a spectral window where coefficients are mutually dependent. From Eq. 9, an ETP coefficient of degree n depends on the coefficients of degree $n - 2j_{max} \leq n \leq n + 2j_{max}$ of the topographic height function.

In a somewhat simpler spherical approach, the geometric heights bounding the mass-layers are mapped onto the surface of a reference sphere (cf. Rexer et al. 2016, Tenzer et al. 2010). This is achieved by introducing a reference sphere instead of a reference ellipsoid for the description of the layer boundaries, leading to the spherical topographic potential (STP). Starting from Eqs. (9-10), the transition from the ETP to the STP is done by applying a constant reference radius ($r_e = R$) and by

setting $e^2 = 0$, i.e. $b = R$. Then the spherical harmonic coefficients of the STP can be written as follows

$$\bar{V}_{nm}^{STP} = \frac{3}{\bar{\rho}(2n+1)(n+3)} \sum_{k=1}^{k_{max}} \binom{n+3}{k} \sum_{\omega=1}^{\omega_{max}} \overline{HDF}_{knm}^{(STP, \Omega_\omega)} \tag{11}$$

where the fully normalised coefficients of the height density function are given by

$$\overline{HDF}_{knm}^{(STP, \Omega_\omega)} = \frac{1}{4\pi} \int_{\lambda=0}^{2\pi} \int_{\varphi=0}^{\pi} \rho^{(\Omega_\omega)} \left(\left(\frac{H_{UB}^{(\Omega_\omega)}}{R} \right)^k - \left(\frac{H_{LB}^{(\Omega_\omega)}}{R} \right)^k \right) \bar{Y}_{nm}(\varphi, \lambda) \, \sin\varphi \, d\varphi d\lambda, \tag{12}$$

and H is the orthometric height. For full details of the forward modelling and the interpretation of the differences between $\bar{V}_{nm}^{STP}$ and $\bar{V}_{nm}^{ETP}$ we also refer to Rexer et al. (2016).

From Eq. (9) [ETP] and Eq. (11) [STP], the topographic potential is expressed as series expansion of integer powers k of the topographic height function.

- If the summation is (deliberately) restricted to k_{max} = 1, the resulting spectral model represents the topographic potential of a Bouguer shell (e.g., Kuhn et al. 2009), which is ellipsoidal in case of Eq. (9) and spherical in case of Eq. (11).
- Evaluation of the series for $2 \leq k \leq k_{max}$ yields a spectral model that represents the terrain correction (i.e., the gravitational effect of all masses residual to the Bouguer shell), cf. Wieczorek (2015).

Both components together (i.e., Bouguer shell plus terrain correction; i.e., $1 \leq k \leq k_{max}$) provide a complete description of the topographic potential in the spectral domain.

3.2 Spherical transform of GGMs

For any study establishing the correlation between topographic and gravitational potential models in the spectral domain, it is important that both models are based on a comparable level of approximation and on the same kind of harmonic representation (e.g., either SHCs or EHCs, but no mixture).

In the literature (Section 6), comparisons of [ellipsoidal] gravitational potential models with STP can be found, resulting in declining correlation at high degree, revealing the underlying levels of approximation to be incompatible (cf. Claessens and Hirt 2013). Generally, for a meaningful spectral comparison with a global gravity model, the spherical approximation should be avoided by using the ETP instead (Claessens and Hirt 2013), thus ensuring comparable levels of approximation.

However, to compare STP models to GGMs, an alternative approach can be taken, by transforming the GGM to the same level of approximation as the STP model. This means that the transformed GGM, here called a 'spherical GGM', should describe the gravitational potential field as it would be if the Earth is morphed into the spherical shape used in the STP, as described above. Strictly, this is not something that can be done exactly without a clear definition describing the movement of the Earth's internal masses in the morphing process. There is, however, a simple transformation that can be used and will prove sufficient given the dominance of the topographic component in the description of the high-degree gravitational potential (cf. Sect. 2.1).

The key is to consider the reference surfaces that the topography and the spherical harmonic coefficients refer to. The spherical harmonic coefficients of an STP model describe the power of the topographic potential on a sphere with a radius equal to the reference radius of the harmonic expansion. This is customarily the same sphere that the topography is assumed to reside on, and it is typically set equal to the semi-major axis of the reference ellipsoid. The spherical harmonic coefficients of a GGM describe the power of the gravitational potential on the same sphere, but the power in the high degrees is lower because near the poles the actual topography is ~21 km below this reference sphere.

Therefore, perhaps paradoxically, a 'spherical GGM' will need to be a set of spherical harmonic coefficients with respect to the reference ellipsoid instead of the reference sphere. Then, both the STP model and the 'spherical GGM' have a situation where the topography resides on the reference surface, and both models will have similar power in the high degrees.

To achieve this situation, the solid spherical harmonic coefficients of the GGM can be transformed to surface SHCs with respect to a reference ellipsoid using a transformation described in Claessens and Featherstone (2008) and Claessens (2016). This results in SHCs of the 'spherical GGM', here denoted $\bar{V}_{nm}^{sph}$

$$\bar{V}_{nm}^{sph} = \sum_{i=-\infty}^{\infty} \sum_{j=|i|}^{\infty} \alpha_{n-2i,j} K_{n-2i,m}^{ij} \bar{V}_{n-2i,m} \qquad (13)$$

where

$$\alpha_{nj} = \left(\frac{R}{b}\right)^{n+1} (-1)^j \binom{\frac{n+1}{2}}{j} e^{2j} \qquad (14)$$

and $K_{n-2i,m}^{ij}$ are the fully normalised sinusoidal Legendre weight functions (see Claessens 2005 for full equations).

Note that there is an ellipsoidal surface behind the coefficients in Eqs. (13) and (14). This is because any transformation from ellipsoidal to spherical approximation will necessarily require parameters that define the shape of the original ellipsoidal surface with respect to which the original ellipsoidal mass arrangement was defined. Both infinite summations in Eq. (13) always converge, and they converge rapidly when the reference ellipsoid is near-spherical.

The coefficients in Eq. (13) are referred to as spherical, because they describe the potential at the spherical approximation level (mass arrangement relative to a sphere). The resulting spherical harmonic model is therefore considered a 'spherical GGM' for the purpose of a spectral comparison with STP models.

3.3 Correlation measures

To quantify the relation between gravitational and topographic potential in the spectral domain, we use the two indicators degree correlation coefficients and signal reduction rates. Both indicators are computed from the potential coefficients as a function of the harmonic degree and are somewhat complementary.

3.3.1 Degree correlation coefficients (CCs)

For a given harmonic degree n, the correlation coefficient between the harmonic coefficients $\bar{V}_{nm}^{A}$ and $\bar{V}_{nm}^{B}$ is obtained via

$$CC_n = \frac{\text{cov}_n\left(\bar{V}_{nm}^A, \bar{V}_{nm}^B\right)}{s_n(\bar{V}_{nm}^A) \cdot s_n(\bar{V}_{nm}^B)} \tag{15}$$

whereby $\bar{V}_{nm}^A$ represents the gravitational potential and $\bar{V}_{nm}^B$ the topographic potential. The correlation coefficient from Eq. (15) follows the definition of Bravais-Pearson, is dimensionless, and meets the relation $-1 \leq CC_n \leq +1$. The degree covariance is obtained from

$$\text{cov}_n = \frac{1}{2n+1} \sum_{m=-n}^{n} (\bar{V}_{nm}^A - \overline{\bar{V}_n^A})(\bar{V}_{nm}^B - \overline{\bar{V}_n^B}) \tag{16}$$

and the degree standard deviation via

$$s_n(\bar{V}_{nm}^A) = \sqrt{\frac{1}{2n+1} \sum_{m=-n}^{n} (\bar{V}_{nm}^A - \overline{\bar{V}_n^A})^2} \tag{17}$$

$$s_n(\bar{V}_{nm}^B) = \sqrt{\frac{1}{2n+1} \sum_{m=-n}^{n} (\bar{V}_{nm}^B - \overline{\bar{V}_n^B})^2} \tag{18}$$

where $\overline{\bar{V}_n^A}$ or $\overline{\bar{V}_n^B}$ are the mean values (arithmetic averages) of the $\bar{V}_{nm}^A$ or $\bar{V}_{nm}^B$ per degree. Correlation coefficients are widely used in the literature, e.g., Konopliv et al. (1999), McGovern (2002), Chambat and Valette (2005), Novak (2010), Zuber et al. (2013), Konopliv et al. (2013), Tsoulis and Patlakis (2013), Lemoine et al. (2014), Wieczorek (2015), to quantify the relation between the gravitational and topographic potential. The degree correlation coefficient can be thought of as a measure of "similarity" between the coefficients of the two potential fields A and B for a given degree.

An inherent weakness of the degree correlation is its invariance against any degree scale factor different from zero. In other words, it cannot sense scale differences between the two coefficient sets involved (e.g., Hirt et al. 2012, Tsoulis and Patlakis 2013). This can be of relevance, for instance, when one of the models is underpowered. The locations of the gravity highs and lows implied by the $\bar{V}_{nm}^A$ and $\bar{V}_{nm}^B$ coefficients would still be the same, but the signal strengths be different (Hirt et al. 2012). Thus, "*even if a high correlation by degree exists, the two models may still differ by a dominant scale factor*" (Tsoulis and Patlakis 2013, p203), and can be in significant disagreement. A remedy to this problem is the use of signal reduction rates.

3.3.2 Signal reduction rates (RRs)

For a given harmonic degree, signal reduction rates quantify the extent to which the signal strength associated with $\bar{V}_{nm}^A$ is reduced by subtracting $\bar{V}_{nm}^B$ from $\bar{V}_{nm}^A$. Compared to correlation coefficients, reduction rates are sensitive to scale differences between the model coefficients, and are therefore an important complementary indicator that is included in our study. To compute signal reduction rates from the harmonic model coefficients of degree n, we adopt the spatial-domain definition of RRs from Hirt et al. (2012) to potential coefficients:

$$RR_n = 100\%(1 - \frac{RMS(\bar{V}_{nm}^A - \bar{V}_{nm}^B)}{RMS(\bar{V}_{nm}^A)}) \tag{19}$$

where RMS is the root-mean square operator, applied on the coefficient differences $\bar{V}_{nm}^A - \bar{V}_{nm}^B$ and the coefficients of the reference model $\bar{V}_{nm}^A$. Alternatively to the RMS operator, the standard deviation could be computed, leading to identical RR-values if the mean value of the coefficients (and coefficients differences) for a given degree vanishes. Identical or similar indicators were used, e.g., by Tscherning (1985) for the evaluation of degree-180 gravity field models, by Chambat and Vallette (2005) for a comparison of EGM96 with topographic potential models, by Hirt et al. (2012; 2015) for evaluation of GOCE gravity fields, by Tsoulis and Patlakis (2013) for assessment of various geopotential models, and by Grombein et al. (2016) for comparisons between EGM2008 and topographic potential models.

In this study, we use as reference model the coefficients of the observed gravitational potential $\bar{V}_{nm}^A$. Regarding the interpretation of RRs, negative values indicate that the coefficients of models A and B are not close to each other. Slightly positive RRs (e.g., 10-20 %) demonstrate moderate topography-generated signals ($\bar{V}_{nm}^B$) are present in the $\bar{V}_{nm}^A$ coefficients. Substantial topographic gravity signals contained in the gravitational potential model are indicated by RRs around 50-60%. RRs cannot exceed 100% and do usually not get close to that value because of model and data errors, and unknown mass-density anomalies reflected by the observed potential, but not contained in the topographic potential (e.g., Hirt et al. 2012).

4 Data

4.1 Gravitational potential models

As high-resolution spectral models of the Earth's gravitational potential, we use the EGM2008 (Pavlis et al. 2012) and EIGEN-6C4 (Förste et al. 2015). Both models represent the geopotential as spherical harmonic series expansions to spherical harmonic degree 2190.

The EGM2008 model relies on a combination of GRACE satellite gravity data (defining the long wavelengths) with a global 5 arc-min resolution area mean grid of marine gravity, terrestrial gravity and topography data, as detailed in Pavlis et al. (2012). Compared to EGM2008, the EIGEN-6C4 model incorporates other data sets, e.g., GOCE satellite gravity data (5th-generation model release obtained from the so-called direct approach) combined with newer GRACE data as improved data source for the long and medium wavelengths (say, to 70-80 km spatial scales, or harmonic degree 280), as well as updated marine gravity (2010 release by the DTU) over the oceans. Over land areas, however, Förste et al. (2015) use EGM2008 gravity information beyond the resolution of the satellite gravity data sets in their EIGEN-6C4 model.

The terrestrial gravity data defines the EGM2008 (and, likewise, the EIGEN-6C4) gravity field over land areas with good gravity coverage (Europe, North America, Australia), while topographic gravity (i.e., gravity information implied by a topographic mass model) is used to define the short-scale gravity field over land areas devoid of dense terrestrial gravity information (parts of Asia, Africa and South America). Topographic gravity data from the latter technique, described in detail in Pavlis et al. (2007), is also known as "fill-in", or "synthetic" gravity. According to Pavlis et al. (2013), forward modelling delivered the high-frequency constituents of EGM2008 over the fill-in areas as shown in Fig. 3 in Pavlis et al. (2012) in a spectral window of ellipsoidal harmonic degrees 901 to 2159, which translates into spatial scales of ~25 to ~10 km.

Following Pavlis et al. (2012), the EGM2008 model was developed in terms of EHCs complete to degree and order 2159. The EGM2008 spherical harmonic coefficients (SHCs), which are used by most practitioners and at IAG's ICGEM, were obtained through application of the Jekeli (1988) transformation described in Sect. 2.2. The commonly used EGM2008 spherical harmonic representation features additional SHCs to degree 2190 (but order 2159), which are a result of the

EHC-to-SHC transformation. The differences in gravity field representation associated with SHCs and EHCs play an important role for correlation measures, as will be shown in Sect. 5.

The EGM2008 model to degree 2190 was also transformed into a 'spherical GGM' (here named sphEGM2008) using the method described in Sect. 3.2. The coefficients were obtained via Eq. (13) using the EGM2008 reference ellipsoid parameters. The summation over i in Eq. (13) was evaluated from -40 to 40, and the summation over j to 40. This results in a spherical harmonic model to degree 2270, which is more than sufficient (Claessens 2016).

Table 2 gives an overview of the gravitational potential models used as representations of the "observed" gravitational potential in this study and Fig 2 shows the dimensionless degree variances for all SH models, computed via

$$d_n = \sum_{m=-n}^{n} (\bar{V}_{nm})^2 \tag{20}$$

Figure 2 shows a grouping of the degree variance spectra (of all models used in this study). One group comprises the spectra of models based on ellipsoidal approximation, while the other the spectra of those based on spherical approximation (also see Rexer and Hirt 2015). For degree variances computation from EHCs and interpretation see also the discussion in Lowes and Winch (2012).
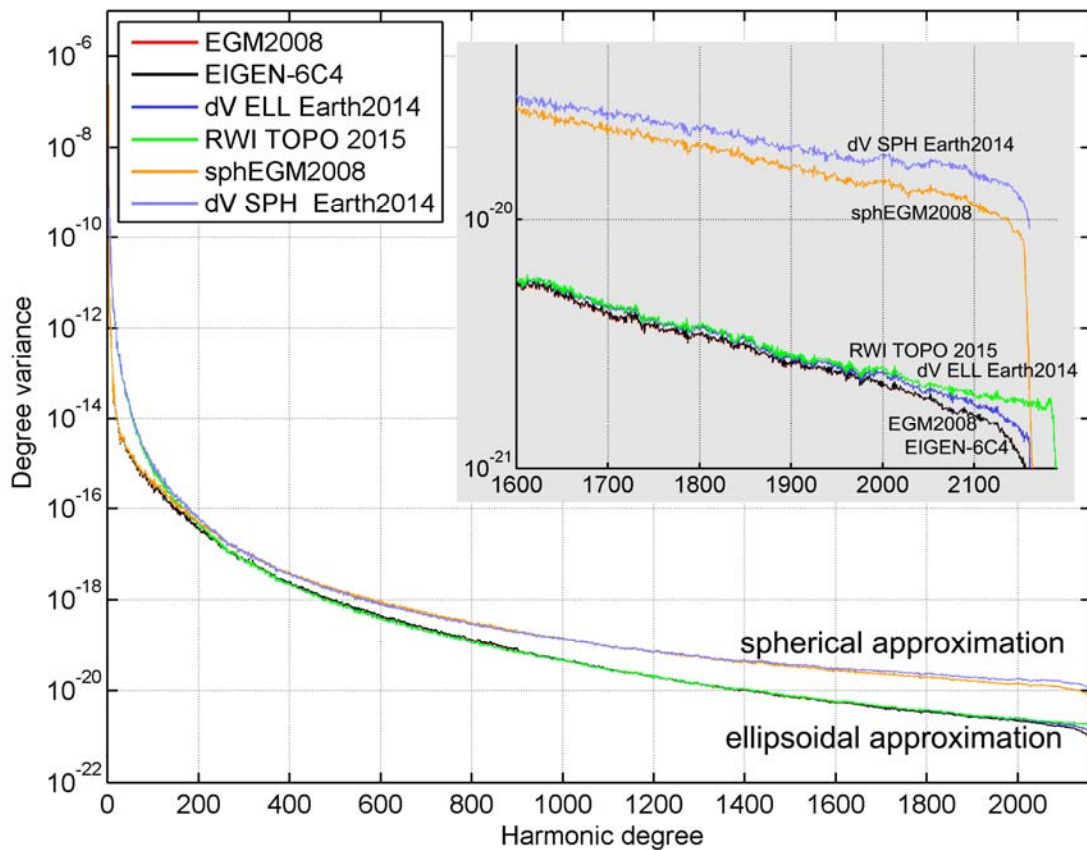

Fig. 2 Dimensionless degree variances as a function of the harmonic degree for the spherical harmonic models of the gravitational potential (EGM2008, sphEGM2008 and EIGEN-6C4) and of the topographic potential (dV_ELL_Earth2014, dV_SPH_Earth2014, RWI TOPO 2015) used in this study. The figure shows the grouping of the models based on spherical approximation (sphEGM2008, dV_SPH_Earth2014) and based on ellipsoidal approximation (EGM2008, EIGEN-6C4, dV_ELL_Earth2014, RWI_TOPO_2015)

Tab. 2 Overview of gravitational and topographic potential models used in this study

Model	Type	Harmonic Coefficients	Earth mass approximation	Source
EGM2008	Gravitational potential	SHCs to 2190	Ellipsoidal	ICGEM
	Gravitational potential	EHCs to 2159	Ellipsoidal	Eq. 6
sphEGM2008	Gravitational potential	SHCs to 2270	Spherical	DDFE, Eq. 13
EIGEN-6C4	Gravitational potential	SHCs to 2190	Ellipsoidal	ICGEM
dV_ELL_Earth2014	Topographic potential	SHCs to 2190	Ellipsoidal	ICGEM, Eq. 9
	Topographic potential	EHCs to 2159	Ellipsoidal	Eq. 6
dV_SPH_Earth2014	Topographic potential	SHCs to 2160	Spherical	DDFE, Eq. 11
RWI_TOPO_2015	Topographic potential	SHCs to 2190	Ellipsoidal	ICGEM
dV_ELL_RET2014	Topographic potential, RET mass-compression	SHCs to 2190	Ellipsoidal	DDFE
dV_SPH_RET2014	Topographic potential, RET mass-compression	SHCs to 2160	Spherical	DDFE

ICGEM = model coefficients available via http://icgem.gfz-potsdam.de/ICGEM/; DDFE = model coefficients available via Curtin University's DDFE server http://ddfe.curtin.edu.au/models/

Tab. 3 Overview of models of the mass-layers (constituents) of the topographic potential

Model	Description	Density (kg m^{-3})	Lower bound	Upper bound
dV_SPH_CRUST2014	Topographic potential of Earth's crust (topography over land, bathymetry over the oceans, bedrock over Antarctica, Greenland)	2670	REF	BED
dV_SPH_LAND2014	Topographic potential of Earth's land masses (topography over land, zero heights over oceans)	2670	REF	SUR
dV_SPH_BATHY2014	Topographic potential of Earth's seafloor relief (bathymetric depths over oceans, zero heights over land)	2670	REF	BED
dV_SPH_OCEAN2014	Topographic potential of the ocean water masses (outside oceans: LB = UB = SUR-ICE)	1030	BED	SUR-ICE
dV_SPH_ICE2014	Topographic potential of the ice sheets (outside ice: LB = UB = SUR-ICE)	917	SUR-ICE	SUR
dV_SPH_LAKES2014	Topographic potential of major lakes (outside lakes: LB = UB = SUR-ICE)	1000	BED	SUR-ICE

All constituents of the topographic potential modelled in spherical approximation. LB: lower bound, UB: upper bound, REF = reference surface used in the topographic potential modelling, SUR: Earth2014 surface layer, BED: Earth2014 bedrock layer, ICE: Earth2014 ice layer, SUR-ICE: Earth2014 physical surface without ice sheet

heights. All topographic potential coefficients are available via
http://ddfe.curtin.edu.au/models/Earth2014/potential_model/.

4.2 Topographic potential models

This study uses spectral models of the topographic potential developed based on the 1-arcmin resolution Earth2014 global relief model (Hirt and Rexer 2015), which is available via http://ddfe.curtin.edu.au/models/Earth2014/. Earth2014 provides grids and surface spherical harmonic coefficients describing the topography (over land areas), bathymetry (over the oceans and major lakes), and thickness of ice-sheets (over Greenland and Antarctica) based on recent data sets available in early 2014. These include Version9 SRTM30_PLUS (Becker et al. 2009), SRTM V4.1 (Jarvis et al. 2008), Greenland Bedrock Topography (Bamber et al. 2013), and the Bedmap2 product (Fretwell et al. 2013) over Antarctica.

Importantly, the Earth2014 topography layers can be used to accurately define the upper bound (UB) and lower bound (LB) of water bodies (ocean and inland lakes), ice-sheets and of the visible land topography (bounded by the geoid). Together with an appropriate mass-density value, the LB and UB define a mass-layer. The implied topographic potential of a single mass-layer can be computed with the formalism described in Sect. 3.1. Following the superposition principle of gravity forward modelling (e.g. Blakely 1996), the (complete) topographic potential of the topographic, water and ice masses is obtained through addition of the potential of the single mass layers. This principle has been applied in the construction of the topographic potential model dV_ELL_Earth2014 and its spherical "sister-model" dV_SPH_Earth2014 (Rexer et al. 2016). While the first models Earth's topographic potential relative to a mass-ellipsoid ("ELL"), the latter uses a mass-sphere ("SPH") as the reference (also see Sect. 3 and Table 2).

In addition to the "complete" models (in the sense of representing the gravitational effect of topography, water and ice masses through a single set of coefficients) of the topographic potential, we also compute correlations between the gravitational potential and the single mass-layer models (i.e., the constituents of the topographic potential). The mass-layers describe the topographic potential associated with (1) Earth's crust dV_SPH_CRUST2014, (2) Earth's land topography only dV_SPH_LAND2014, (3 Earth's bathymetric bedrock only dV_SPH_BATHY2014, (4) Earth's ocean water masses dV_SPH_OCEAN2014, (5) Earth's ice masses dV_SPH_ICE2014, and (6) Earth's lake water masses dV_SPH_LAKES2014. Table 3 provides computational details (adopted mass-density values, definition of upper and lower bounds and treatment of data away from the modelled mass layer). All mass-layers are modelled in spherical approximation complete to degree and order 2160. Note that the models 1 and 3 to 6 are based on the so-called layer correction approach, while model 2 is based on the layer reduction approach (for full details cf. Rexer et al. 2016, Sect. 3 ibid). The dimensionless degree variances of six five mass-layer models are shown in Fig. 3.

Further, we include two additional topographic potential models (dV_ELL_RET2014 and dV_SPH_RET2014) in this study. These two models do not use multiple mass-layers to model the topographic potential; instead they rely on the so-called concept of rock-equivalent topography (RET, cf. Lee and Kaula 1967, Rummel et al. 1988, Wieczorek 2015). In the RET-concept, anomalous masses (mostly ice and water masses) are mathematically compressed to rock, such that the topographic potential can be modelled based on a single mass layer and a single constant mass-density (mostly that of topographic rock). The advantage of the RET concept is that the modelling is somewhat simplified. A disadvantage is that the location and geometry of the masses are changed through mathematical compression, resulting in approximation errors (Kuhn and Hirt 2016; Grombein et al. 2016). The dV_ELL_RET2014 and dV_SPH_RET2014 models are included in order to show the effect of the RET-compression on correlation coefficients, both in spherical and in ellipsoidal

approximation. Both models use the Earth2014 rock-equivalent topography layer RET2014 as only input layer, full details on the construction of RET2014 are found in Hirt and Rexer (2015, appendix A).
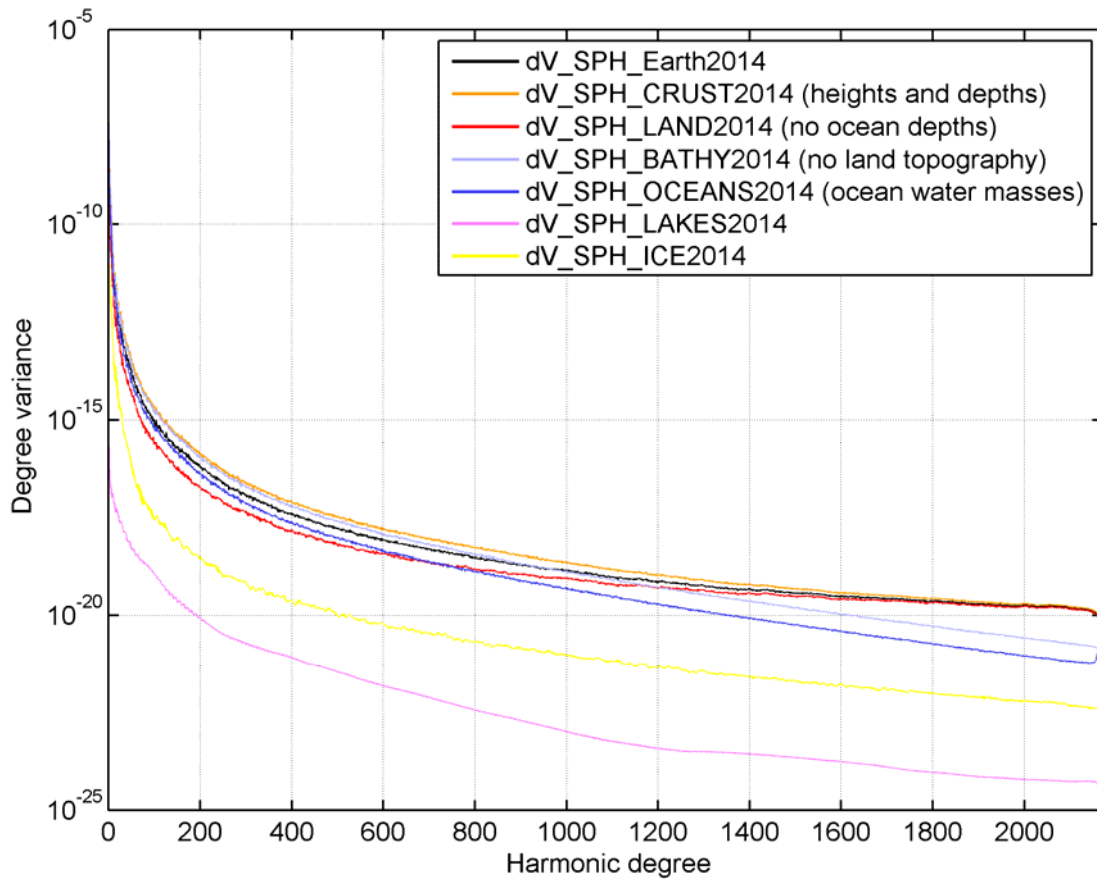

Fig. 3 Dimensionless degree variances as a function of the harmonic degree for the spherical topographic potential model dV_SPH_Earth2014 (modelled with 3D mass layers) and the implied potential of the model constituents crust (heights over land, depths over oceans), land topography only (no ocean depths), crustal ocean bathymetry (no land topography), ocean water masses (here modelled as density constrast of 1030-2670 kg m^{-3}), Earth's major lakes and ice-masses of Antartica and Greenland.

Finally, we include the topographic potential model RWI_TOPO_2015 (Grombein et al. 2016), developed with an independent computational approach. The RWI_TOPO_2015 model uses the Earth2014 topographic mass model as input data, too. Following Grombein et al. (2016), in RWI_TOPO_2015, the gravity forward modelling was done in the spatial domain, by computing high-resolution global grids of topographic potential values implied by (1) topographic rock, (2) water masses, and (3) ice masses, using tesseroids as mass elements and evaluating the gravitational signal at some constant height above the reference ellipsoid. A subsequent spherical harmonic analysis of the gridded potential values was used to obtain the SHCs to degree 2,190 or higher (cf. Grombein et al. 2016 for full details).

The dV_ELL_Earth2014 (Rexer et al. 2016) and RWI_TOPO_2015 (Grombein et al. 2016) are very similar in that they use the same input topographic mass model (Earth2014), represent the topographic potential in ellipsoidal approximation (relative to the GRS80 mass ellipsoid), use mass layer representations to avoid approximation errors associated with RET, and provide a degree-2190 or 5 arc-min spatial resolution for the topographic potential. As a consequence of the ellipsoidal

approximation level applied in both models, the potential coefficients in band of degrees 2,160-2,190 are crucially important to avoid artefacts (striations) in gravity syntheses in high-latitudes (see Claessens and Hirt 2013, Sect 3 ibid; Rexer et al. 2016, Sect. 4.3; Grombein et al. 2016; Sect. 4). As for the difference between the two models, dV_ELL_Earth2014 solely relies on spectral-domain forward modelling, whereas the RWI_TOPO_2015 model is based on spatial-domain forward modelling as an intermediate step prior to the generation of the model coefficients through SHA. The differences between the two models are thus primarily due to different computational procedures, and their effect on correlation measures is studied in Sect 5.6.

The spectra of all topographic potential models are shown together with those of the gravitational potential models in Fig. 2. Note that the grouping of spectra primarily reflects the underlying approximation level (spherical vs. ellipsoidal approximation) and not the potential model type (gravitational vs. topographic potential).

5. Numerical results

5.1 General observations

The general behaviour of correlation measures between the Earth's gravitational and topographic potential is known from previous studies (e.g., Claessens and Hirt 2013; Wieczorek 2015, Hirt et al. 2015, Grombein et al. 2016, Rexer et al. 2016). From Fig. 1, the degree correlation assumes low values (say below +0.5) for low harmonic degrees (n<10) and increases to values between +0.6 and +0.8 for 50<n<200. This well-known behaviour indicates the presence of significant mass anomalies (e.g., neglected isostatic compensation masses, deep interior anomalies) that affect the long-wavelength constituents of the gravitational potential (e.g., Watts 2011).

For 200 <n<2160, the CCs show varying behaviour (cf. Fig. 1), depending on the underlying approximations that are studied and discussed in detail in Sect. 5.1 and 5.2. All curves show a jump-like increase in CC at n=900, which reflects the use of fill-in data in EGM2008 at spatial scales less than ~27 km (cf. Pavlis et al. 2013).

When the topographic and gravitational potential models are based on the same approximation level, CCs increase to the level of +0.9. When the models involved are incompatible (e.g., topographic potential modelled in spherical approximation, gravitational potential based on ellipsoidal approximation), there is a spurious decline in correlation visible beyond degree ~400. This is seen by the magenta curve in Fig. 1.

The lowest correlations at high degrees are observed among the coefficients of the topography (*not potential*) and those of the gravitational potential, reflecting the non-linear relation between topography and implied potential. However, at low harmonic degrees a linear approximation offers similar correlation values as a complete model of the topographic potential (Sect. 5.5).

5.2 Spherical vs. ellipsoidal approximation and spherical vs. ellipsoidal harmonics

Figure 4a shows the degree correlation coefficients (CCs) computed between the EGM2008 gravitational potential model and the Earth2014-based topographic potential model in three variants.

- Case A: CCs between the SHCs of the two models EGM2008 and dV_ELL_Earth2014, as can be obtained via IAG's ICGEM.
- Case B: CCs between the EHCs of the two models EGM2008 and dV_ELL_Earth2014. The EHCs of both models were computed from the SHCs using the Jekeli (1988) transformation in Eq. 6.

- Case C: CCs between sphEGM2008 (the spherical transform of EGM2008) and the dV_SPH_Earth2014 topographic potential model (instead of the dV_ELL_Earth2014).

Importantly, in each of the three cases the model pairs are based on a comparable level of approximation and on the same kind of harmonic representation (SHC or EHC). Notwithstanding, there are spurious differences visible. In cases A and B, all models involved rely on the ellipsoidal approximation (EA) level, while in case C the geopotential and topographic potential model are based on the spherical approximation (SA) level (see definitions in Sect. 2.3).
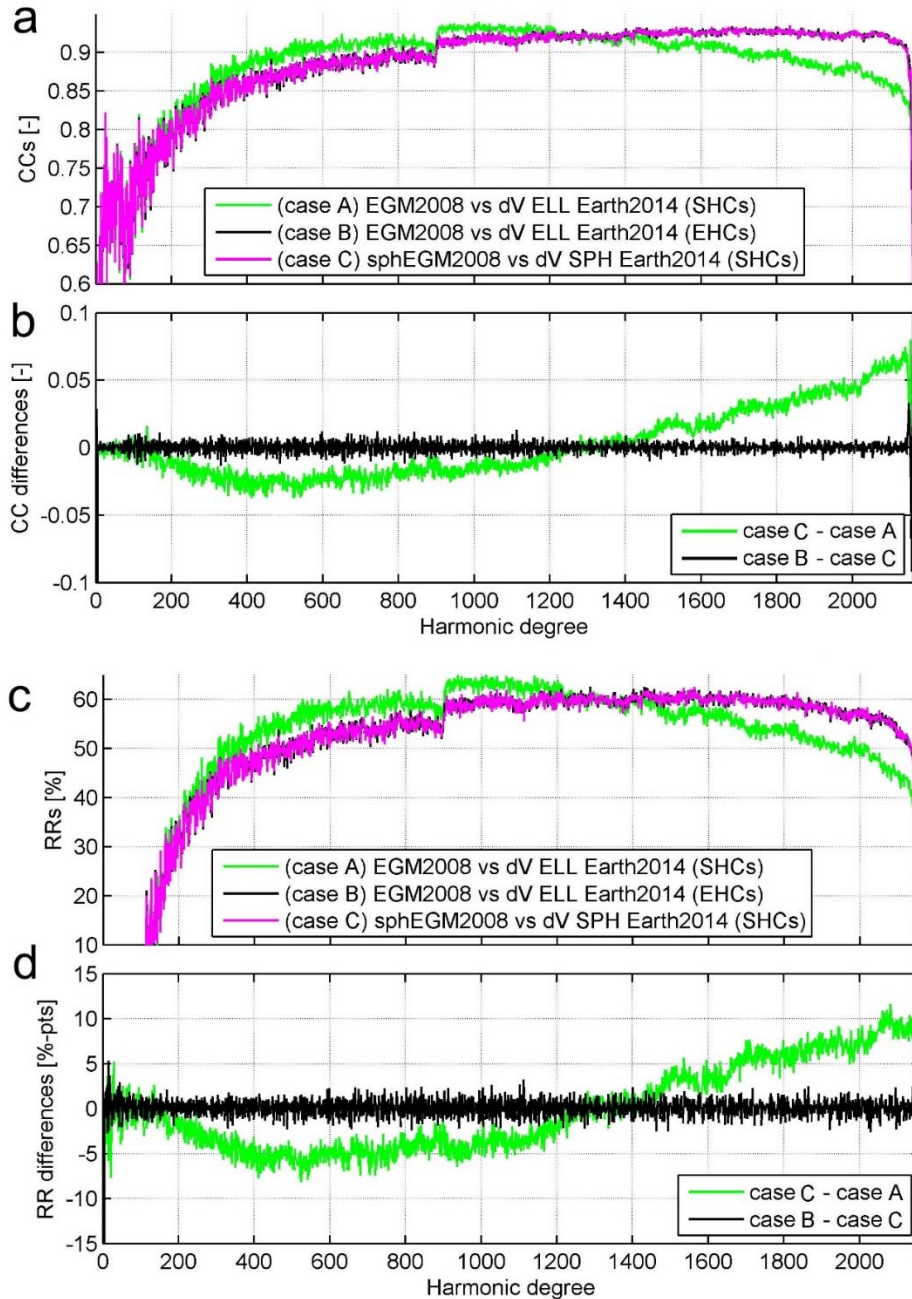
Fig. 4. Panels a,b: Correlation coefficients (CC) in spherical and ellipsoidal approximation and their differences. CC between SHCs of EGM2008 and the ETP (model dV_ELL_Earth2014) in green, between EHCs of EGM2008 and the ETP (model dV_ELL_Earth2014) in black and between SHCs of sphEGM2008 and the STP in magenta. Panels c,d: Signal reduction rates (RRs) in spherical and ellipsoidal approximation and their differences.

Figures 4a and 4b reveal that the CCs of case B (EHCs and EA) and case C (SHCs and SA) are in very close agreement over most of the spectrum. The differences in CCs are mostly at the level of 0.01 or below. Also, RRs (Fig. 4c and 4d) show a close agreement between cases B and C. Opposed to this, the CCs and RRs in case A (SHCs and ellipsoidal approximation) show a contrasting behaviour over most of the spectrum. From degrees ~200 to ~1250, the model pair combination "SHCs and EA" suggests higher correlation (up to 0.03 in terms of CCs and up to 5% in terms of RRs) than cases B/C, while this behaviour reverses at short scales, say from degrees ~1400 to ~2160.

In band of harmonic degrees ~1000-2160 and case A, CCs exhibit a declining behaviour. This is against the expectations. The CCs are considerably lower than that in cases B/C, and the differences exceed a value of 0.05 (Fig. 4b). In terms of RRs, the values are up to 10% lower in case A (Fig. 4d). There is ample evidence that the CCs and RRs in case A are biased, and thus less realistic than the CCs and RRs in cases B/C:

First, in case A, both the gravitational and topographic potential model are represented as SHCs while based on EA. By virtue of the computational procedures used to obtain the SHCs (Eq. 6 for the gravitational potential and Eq. 9 for the topographic potential), both models can only be accurately used over the full band-width, that is, in band of degrees 2 to 2190. Accordingly, band-limited mathematical operations (such as correlation coefficient computation or synthesis of the gravity signals implied by a single harmonic degree n, e.g., 900) are influenced by the "windowing effect" (that is, the dependence of each individual SHC on a spectral bracket of up to 30 input coefficient degrees to either side of n, producing functional correlations, cf. Sect. 2.3 and 3.1). While negligible to degree ~200, the windowing effect plays a crucial role at medium and particularly high harmonic degrees and prevents band-limited operations such as short-scale gravity syntheses, as demonstrated in Appendix A1. Appendix A2 provides a new numerical experiment that reveals the windowing effect to be responsible for introducing biases in CCs and RRs.

Second, case B (EHCs and ellipsoidal approximation) and case C (SHCs and spherical approximation) are based on potential coefficients that are allowed to be evaluated or investigated degree-wise. Importantly, there is no similarly pronounced windowing effect (as in case A) that would falsify the correlation coefficients. As a result, the CCs obtained in cases B and C are in excellent mutual agreement (Fig. 4b), providing additional confidence in the CC curves. The same holds for RRs of cases B/C shown in Fig. 4c and 4d. We acknowledge that for a given harmonic degree n, SHCs and EHCs cannot be exactly compared to each other, manifesting as oscillations of amplitude of ±0.01 in the CC differences, and ±2% in RR differences.

Third, only the cases B and C meet the expectation of a (in good approximation) steadily increasing correlation between the topographic and gravitational potential at short scales, as would be expected from correlation studies of other planetary gravity fields (e.g., Zuber et al. 2013). In case of signal reduction rates, a steady increase with harmonic degree is observed only for cases B and C to high harmonic degrees (the reason for the decline in RRs in band 1600-2160 is discussed in Sect. 5.4), while in case A the RRs are seen to increase to degree ~900 only (Fig. 4c).

- From the previous considerations, we conclude that compatibility among the approximation levels and coefficients is ensured, if the models are either (1) represented as SHCs *and* based on SA, or (2) as EHCs *and* based on EA. Then, biases in correlation measures are avoided.
- Mixed cases (e.g., SHCs and EA) -- the current standard in geodesy and inherent to models distributed via IAG's ICGEM -- inevitably cause biases in the CCs at short scales (Fig, 4, case A) and should be avoided.

In summary, Fig. 4 and appendix A2 demonstrate that correlation between high-resolution ICGEM gravity models and the topographic potential may be biased when computed from spherical harmonic coefficients. This is because the underlying ellipsoidal approximation level introduces dependencies (algebraic correlations) between the SHCs of adjoining degrees, and this effect falsifies the degree correlation measures. A spherical GGM (as obtained from Eq. 13) avoids this problem. The transformation described in Eq. 13 removes the algebraic correlations from the SHCs. As a result, biases in the degree correlation measures (as computed from SHCs) are avoided.

In the sequel, we use mixed cases only when reproducing literature results. Otherwise in the next sections correlation measures are computed from the (1) SHCs when the models are based on SA, or (2) EHCs when the models are based on EA.

5.3 RET mass compression

In order to investigate the effect of the RET mass-compression sometimes used in topographic potential modelling (e.g., in Rummel et al. 1988, Hirt et al. 2012, Wieczorek 2015), Fig. 5a compares CCs between a) sphEGM2008 and the dV_SPH_Earth2014 topographic potential model (rigorous layer-based mass modelling) and b) sphEGM2008 and the dV_SPH_RET2014 model (RET compression). As argued before, the models compared are based on SHCs and SA, ensuring mutual compatibility. From Fig. 5a (blue vs. red curve), the CC curves cannot be distinguished to about degree 900, while the CC values exhibit slight differences in the high harmonic degrees. Beyond degree 1400, the CCs are about 0.01 smaller when using the RET compression instead of 3D mass modelling.

Figure 5b shows the same comparison in terms of RRs. Practically over the whole spectrum, RRs are found to be larger or substantially larger when the layer-based forward modelling is used instead of the RET compression in the construction of the topographic potential model. In spectral band of degrees ~1000 to ~2000, RRs are 4-5 %-points smaller for the RET-based topographic potential model, showing that the 3D layer-based forward modelling explains a larger percentage of the short-scale geopotential constituents than the RET-based modelling variant. For instance at degree 1200, 61% of the geopotential is forward-modelled by the dV_SPH_Earth2014 compared to ~56% when dV_SPH_RET2014 is used.

For the sake of completeness, Fig. 5 shows CCs and RRs also when the model SHCs are based on EA, which is the case for EGM2008 vs. dV_ELL_Earth2014 (green curve), and EGM2008 vs. dV_ELL_RET2014 (black curve). The correlation measures are in close agreement to results from a similar analysis presented by Grombein et al. (2016). Compared to the models based on SHCs and SA (red and blue curve), the RET compression effect is more pronounced for the models based on SHCs and EA (green and black curve), e.g., the effect of RET-compression reaches 5-7%-points at short scales, but is subject to biases (cf. Sect. 5.2 and Appendix A2).

The cross comparison between CCs and RRs in Fig. 5a and 5b demonstrates the effect of scale differences on RRs. Particularly the RRs (but to a lesser extent also the CCs) confirm the expectation that topographic potential models are closer to the gravitational potential when a mass-layer (3D) forward-modelling is performed. All in all, the comparisons presented in Fig. 5 corroborate the benefits of 3D forward modelling compared to RET mass compression.
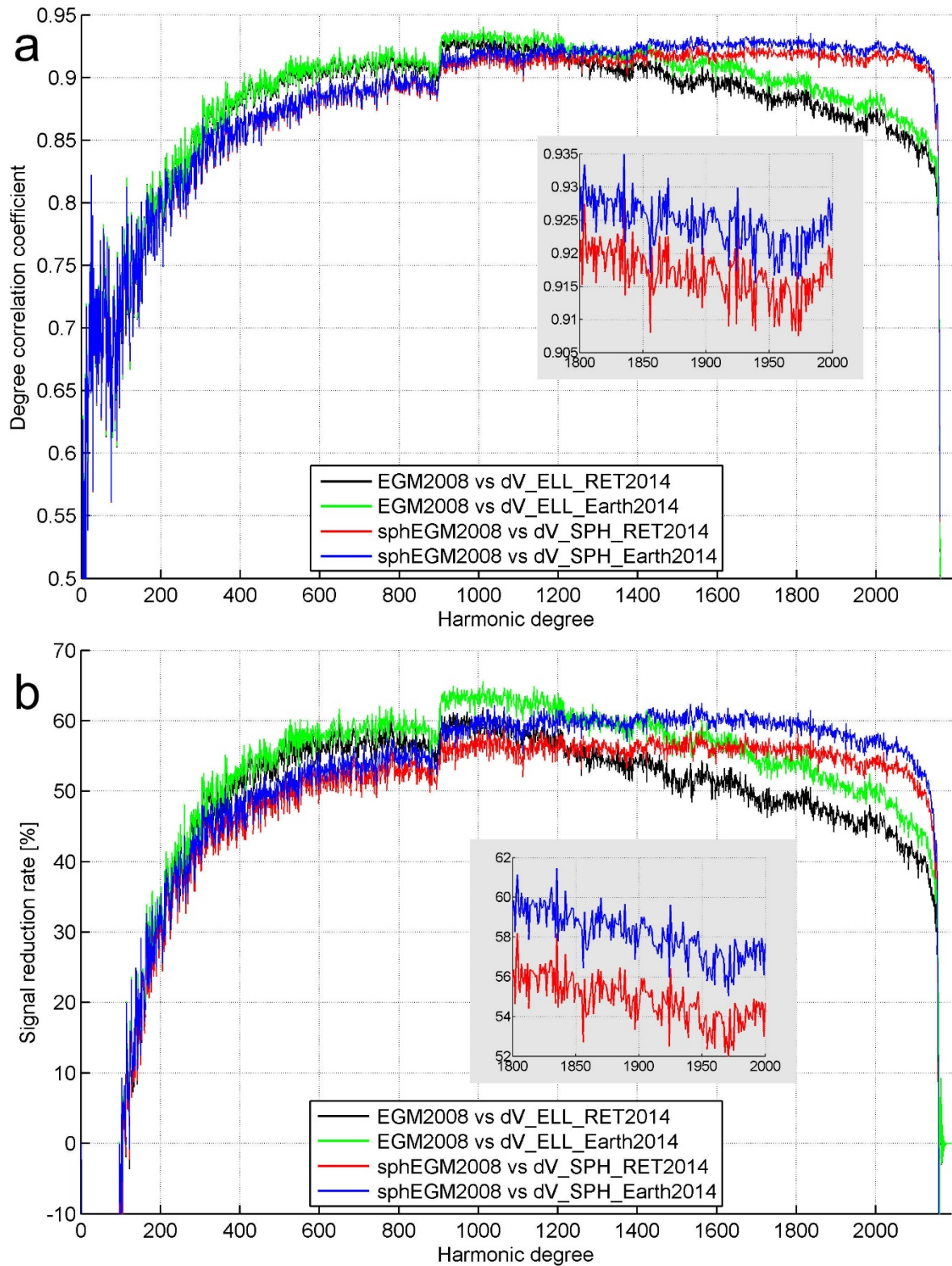
Fig. 5. Approximation effects in correlation measures. Top: correlation coefficients, Bottom: reduction rates. The figure shows the effect of spherical vs. ellipsoidal approximation (blue vs. green and red vs. black curve) and RET vs. 3D mass-layer modelling (blue vs. red and green vs. black) on correlation measures. The highest agreement at short scales (beyond degree 1800) is obtained for spherical approximation and 3D mass layer-modelling (blue curve). All models rely on SHCs.

5.4 Constituents of the topographic potential

Figure 6 presents the CCs and RRs computed between various constituents of the topographic potential (see Tab. 3) with the sphEGM2008 model representing the geopotential. For the sake of completeness, the comparisons also include the (complete) model dV_SPH_Earth2014 that represents the accumulated effect of the mass layers

- dV_SPH_CRUST2014 (land topography and bathymetry),
- dV_SPH_OCEAN2014 (ocean water masses),
- dV_SPH_ICE2014 (ice sheets) and
- dV_SPH_LAKES2014 (inland lakes).

For comparison purposes, also the potential implied by the land topographic masses only (dV_SPH_LAND2014) and by the ocean bathymetry only (dV_SPH_BATHY2014) is included. The models dV_SPH_LAND2014 and dV_SPH_BATHY2014 can be thought of as constituents of the crustal layer dV_SPH_CRUST2014. All comparisons are based on SHCs and the spherical approximation level, so are not subject to truncation effects (Sect. 5.5) or mass compression effects (Sect. 5.3).

Ice sheets and lake water

Both CCs and RRs show that the potential associated with the ice sheets and inland lakes is unrelated to the geopotential on a global scale. This result is well explained by the small fraction of areas covered by ice or lakes relative to the Earth's surface, along with the global character of the RR and CCs in our study (localized correlation methods might yield different results, but their application is beyond the scope of the numerical study).

Land topography and ocean water

The major constituents of the topographic potential are the land topographic masses (dV_SPH_LAND2014, red curve) and ocean water masses (dV_SPH_OCEAN2014 dark blue curve in Fig. 6).

- The potential implied by land topography shows steadily increasing correlation over most of the spectrum. It explains 10% of the geopotential signals at degree 200, 30% at degree 900 and ~58 % at degree 2000. At short scales, it is the main contributor to the Earth's gravitational potential - as represented through the sphEGM2008 model.
- The potential implied by ocean water is the main contributor to the Earth's gravitational potential up to degree ~600-700, with the largest contribution made in the band of degrees ~400 to 600, where it explains ~30 % of the geopotential signal.
- Importantly, the potential implied by ocean water exhibits a steady decline in correlation and signal reduction beyond degree 600 all the way to degree 2160. At degree 900, around 20 % of geopotential signals are generated by the ocean water layer, at degree 1200 the value reduces to 10%, at degree 1500 to 5 % and beyond degree 2000, the ocean water layer is unrelated with the geopotential (RRs around 0 %, CCs below +0.2).
- In a relative sense, ocean water masses make a larger contribution than the land topographic masses to the gravitational potential in band of degrees ~150 to ~700. Beyond degree ~700, the contribution made by land topography is larger than that of the ocean water masses and beyond degree ~1700. Here, the sphEGM2008 potential signal is explained – almost exclusively – through land topography, while the effect of the ocean water masses on sphEGM2008 diminishes and finally vanishes at these high harmonic degrees.
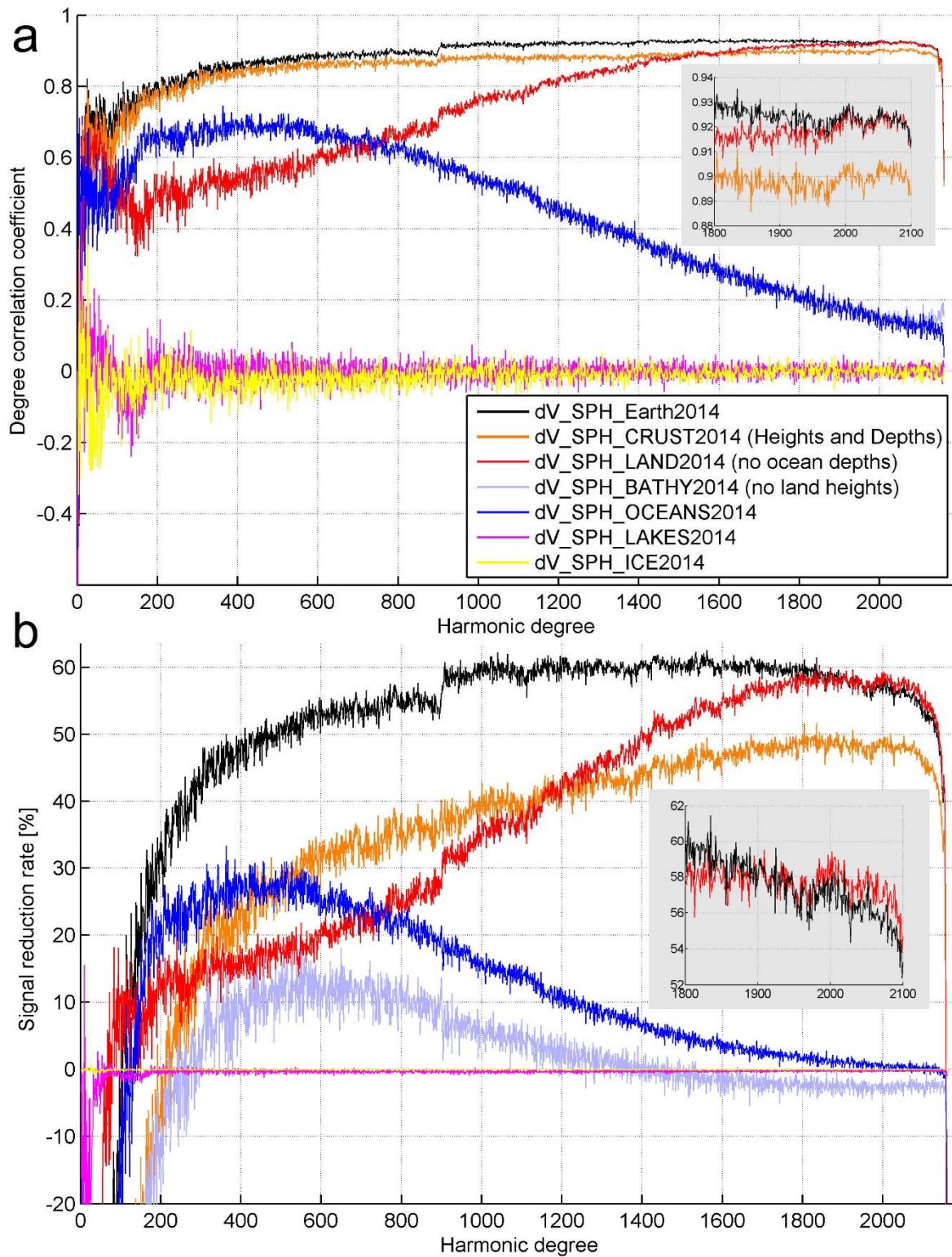
Fig. 6. Top: Correlation between the spherical model sphEGM2008 and the topographic potential model dV_SPH_Earth2014 (black) and its constituents (various colors); Bottom: the same in terms of reduction rates. The top figure shows the correlation between the constituents of the topographic potential with the gravitational potential and the bottom figure shows the amount (percentage) of gravitational signal explained by the topographic potential and its constituents.

Crustal layer and its constituents dV_SPH_LAND2014 and dV_SPH_BATHY2014

We look at the CCs and RRs between the geopotential and the crustal mass-layer model dV_SPH_CRUST2014, and draw a cross-comparison with its crustal constituents i) dV_SPH_LAND2014 (ocean bathymetry = 0) and ii) dV_SPH_BATHY2014 (land topography = 0). Among the three models, dV_SPH_CRUST2014 is the topographic potential constituent offering the highest CC with the gravitational potential over most of the spectrum (orange curve in Fig. 6).

The situation looks different for RRs: In approximation, RRs of dV_SPH_CRUST2014 are the sum of the RRs of its components dV_SPH_BATHY2014 and dV_SPH_LAND2014 (compare orange, red and light blue curves). For dV_SPH_CRUST2014, RRs are negative up to degree ~200, showing that the crustal model alone (without the water mass layers) does not smooth the geopotential signal. However, when the ocean water masses are taken into account, too, RRs rise to values of ~30 % at degree 200 (black curve in Fig 6). The RRs associated with the crustal constituents dV_SPH_LAND2014 are larger than those for dV_SPH_CRUST2014 beyond degree ~1200 (orange vs. red curve), and RRs associated with dV_SPH_BATHY2014 are smaller than those for dV_SPH_LAND2014 over the entire spectrum. The dV_SPH_BATHY2014 model explains a small portion of geopotential signals (up to ~10-15 % around degree 600). Negative RR-values beyond degree ~1500 point at deficiencies in the marine data sets (see discussion below).

Interpretation of the correlation between ocean water and gravitational potential

The perhaps most surprising observation made in Fig. 6 is the vanishing correlation between the potential implied by the ocean water masses (or crustal bedrock over the oceans) and the gravitational potential at short spatial scales. Our correlation and signal reduction analyses show that the marine gravity from altimetry (used in EGM2008, and in turn in sphEGM2008) and gravity obtained through forward-modelling from bathymetry are largely unrelated at 5-6 arc-min spatial scales (or harmonic degrees of ~1800 to ~2160). This suggests that either the marine gravity field, or the global bathymetry, or even both (considering the fact that altimetry observations are the source of marine gravity and also a main source of bathymetry, cf. Becker et al. 2009) are underpowered at 5-6 arc-min scales. Also, the slowly declining correlation between the gravitational and ocean water potentials beyond degree ~600 (18 arc-min scales) suggests that at least one of the two models involved does not offer full signal resolution over the oceans.

According to Pavlis et al. (2012), the Scripps Institution of Oceanography (SIO) v18.1 marine gravity product, a predecessor of the model described in Sandwell and Smith (2009), has been used for EGM2008 over the open oceans, while the Danish National Space Centre DNSC07 marine gravity product, a predecessor or the DNSC08 product described in Andersen et al. (2010) along coastlines.

Sandwell and Smith (2009) present power spectra of the sea surface heights derived from altimetry (Fig. 2 ibid), their input data for the development of the marine gravity grids. From Sandwell and Smith (2009), the signal-to-noise ratio of the sea surface heights equals 1 at about ~24 km resolution, and deteriorates at shorter scales. Andersen (2010) presented a coherence analysis showing the agreement between DNSC08 marine gravity and (higher-resolution) ship-track gravity data, showing full coherence between marine and ship-track gravity data only for wavelengths of 50 km or longer, (= 14 arc-min resolution or degree ~800) and a rapid loss in coherence starting at ~25 km wavelengths (= 7 arc-min resolution or degree ~1600). These independent literature results are in reasonable agreement with our correlation analysis (Fig. 9), in that they holistically demonstrate that the marine gravity fields used to define the short-scale ocean signals in EGM2008 do not offer full resolution in the high harmonic degrees.

We note that the RRs between the topographic potential model dV_SPH_Earth2014 and sphEGM2008 reach their maximum not at the full model resolution, but already around degree ~1500 (around ~60% and experience a slow decline to ~58 % and ~55% (at degrees ~2000 and 2100), cf. Fig. 6b. Compared to this, the land topographic potential (dV_SPH_LAND2014) shows a steady increase in agreement with sphEGM2008 to degree ~2000, and – in a relative sense – no such decline in reduction rates in band ~1500-2100. The main difference between dV_SPH_Earth2014 and dV_SPH_LAND2014 are the ocean water masses and the bathymetric bedrock masses modelled in dV_SPH_Earth2014. We therefore conclude that the limited resolution of the marine gravity or bathymetry data prevents the RRs from reaching maximum values near the full model resolution.

Importance of signal reduction rates

We note that around degree 200, the CC values for the crust-only model dV_SPH_CRUST2014 (+0.78) and the complete topographic potential model dV_SPH_Earth2014 (+0.80) are very close together, while the RRs are substantially different (-5% for dV_SPH_CRUST2014 vs. +30% for dV_SPH_Earth2014). Apparently, there is a scale difference related to the lacking ocean water mass effect in the dV_SPH_CRUST2014 layer, the effect of which "overestimates" the potential signals over the oceans.

Another example is found when comparing the CCs and RRs of the components dV_SPH_BATHY2014 (ocean bedrock masses) vs. dV_SPH_OCEANS2014 (ocean water masses). While the CCs are identical over most of the spectrum (light blue and dark blue curves coincide in Fig 6a), the RRs show differences varying between 5 and 15% (Fig 6b) for most degrees. This reflects a scale difference between the two topographic potential constituents (both use the ocean bedrock as a boundary in the layer-based forward modelling, but rely on different mass-density values, cf. Table 3). These examples demonstrate the vital importance of using signal reduction rates as robust indicator in topographic/gravitational potential comparisons.

5.5 GFM truncation effects, Bouguer shell and terrain correction

In order to investigate the role of truncation effects in the gravity forward modelling (GFM), we have generated variants of the dV_SPH_Earth2014 model by evaluating the series expansion in Eqs. (11) and (12) with different k_{max}-values. Model variants were generated for $k_{max} \in [1,2,3,4,5,12]$. The variant with $k_{max} = 1$ corresponds to a spherical Bouguer shell, and the model with $k_{max} = 12$ makes truncation errors negligible (e.g., Rexer et al. 2016). The other variants are topographic potential models of different "spectral completeness", with the truncation error decreasing as the higher-order powers of the topography are taken into account. Finally, a spectral model representing the spherical terrain correction was constructed by evaluating the series expansion with $2 \leq k \leq k_{max} = 12$.

Figure 7a shows the CCs between sphEGM2008 and all variants of the dV_SPH_Earth2014 model. For the six truncations of dV_SPH_Earth2014, in general the CCs are seen to increase with k_{max} and harmonic degree. For $k_{max} = 1$ (spherical Bouguer shell), CCs show the largest differences w.r.t. complete spectral modelling. When the integer powers of the topography are taken into account ($k_{max} > 1$) in the topographic potential modelling, CCs quickly approach those associated with the dV_SPH_Earth2014 model. For $k_{max} > 4$, CCs are indistinguishable over the whole spectrum (compare the zoom in Fig. 7a).

Of interest is a comparison between the CCs of sphEGM2008 with a spherical Bouguer shell (blue curve). Up to degree ~200, the CCs associated with the Bouguer shell are identical with those of the untruncated topographic potential model (black curve). This suggests that – at least at long wavelengths – the Bouguer shell is a decent approximation of the topographic potential, and higher-

order powers are negligible (a similar conclusion can be drawn based on a contribution analysis to the topographic potential in Hirt and Kuhn 2012, Fig. 1 ibid). The CCs between the geopotential and the Bouguer shell decline beyond harmonic degree 600, down to the level of +0.6 at the end of the spectrum. This behaviour demonstrates that the non-linear relationship between topography and implied gravity (Sect. 3.1) becomes increasingly important with increasing spatial resolution of the gravity modelling.

The CC between the geopotential and the terrain correction (grey curve) exceed those of the Bouguer shell beyond degree ~1800, with maximum values (about +0.7) reached near the end of the spectrum, around degree ~2160. A similar comparison in terms of RRs (Fig. 7b) shows that

- The Bouguer shell is a good approximation of the topographic potential to n=200. About 30% of geopotential signals are explained at n=200 by a Bouguer shell alone, and the terrain correction does not improve this value.
- Over large parts of the spectrum, say to degree 1400, the spherical terrain correction is unrelated to the gravitational potential. This is seen from the negative or zero RRs and the insignificant CC values.
- However, at short scales, around degree 2,100, the Bouguer shell explains about 20 % of geopotential signals only, while about 25% is explained by the spherical terrain correction.

Regarding the relation between the sphEGM2008 and the various truncations $k_{max} \in [2,3,4,5,12]$ of the dV_SPH_Earth2014 model, the RRs are largely the same to degree ~900, start to differ beyond that degree, and show quite a surprising behaviour in spectral band ~1900 to ~2160: In this short-scale harmonic band, the highest RRs are not conferred by the most complete spectral model (e.g., $k_{max} = 12$), but by the model variants truncated to $k_{max} = 4$ (compare zoom in Fig. 7b). These truncated models can be thought of as somewhat smoothed representations of the topographic potential because the contributions made by the higher-order powers of the topography are (deliberately) not accounted for.

From a theoretical point of view, there is no reason why a truncated ($k_{max} = 4$) topographic potential model should be superior to a spectrally complete modelling ($k_{max} = 12$), where series convergence is reached (cf. Rexer et al. 2016). Also, a cross-comparison between spectral and spatial domain forward modelling (based on numerical integration) and a one-layer degree-2160 mass model has shown the importance of higher-order powers for a complete representation of the implied gravity signals (Hirt et al. 2016).

Not shown for the sake of brevity, but we have repeated the experiments shown in Fig. 7 with the truncated topographic potential models based on EA, and the correlation measures computed from the EHCs of the models involved (EGM2008 and the topographic potential models). The CCs and RRs computed in EA & EHCs confirm those shown in Fig. 7 (based on SA and SHCs), particularly the best agreement among $k_{max} = 4$ topographic potential models with EGM2008 at short scales. We can therefore exclude the approximative character of the EGM2008 to sphEGM2008 transformation (Sect 3.2) as reason for the short-scale behaviour visible in Fig. 7.

The observation that an "incomplete" spectral topographic potential model ($k_{max} = 4$) offers the best short-scale agreement with sphEGM2008 therefore suggests that EGM2008 or the data used to generate the topographic potential models is marginally underpowered at short spatial scales. However, the effect is fairly small and affects the highest harmonic degrees only. A possible explanation could be that the ocean altimetry or bathymetry values are systematically too smooth at short spatial scales, and that the observed behaviour is a manifestation of that effect (also see discussion in Sect 5.4).
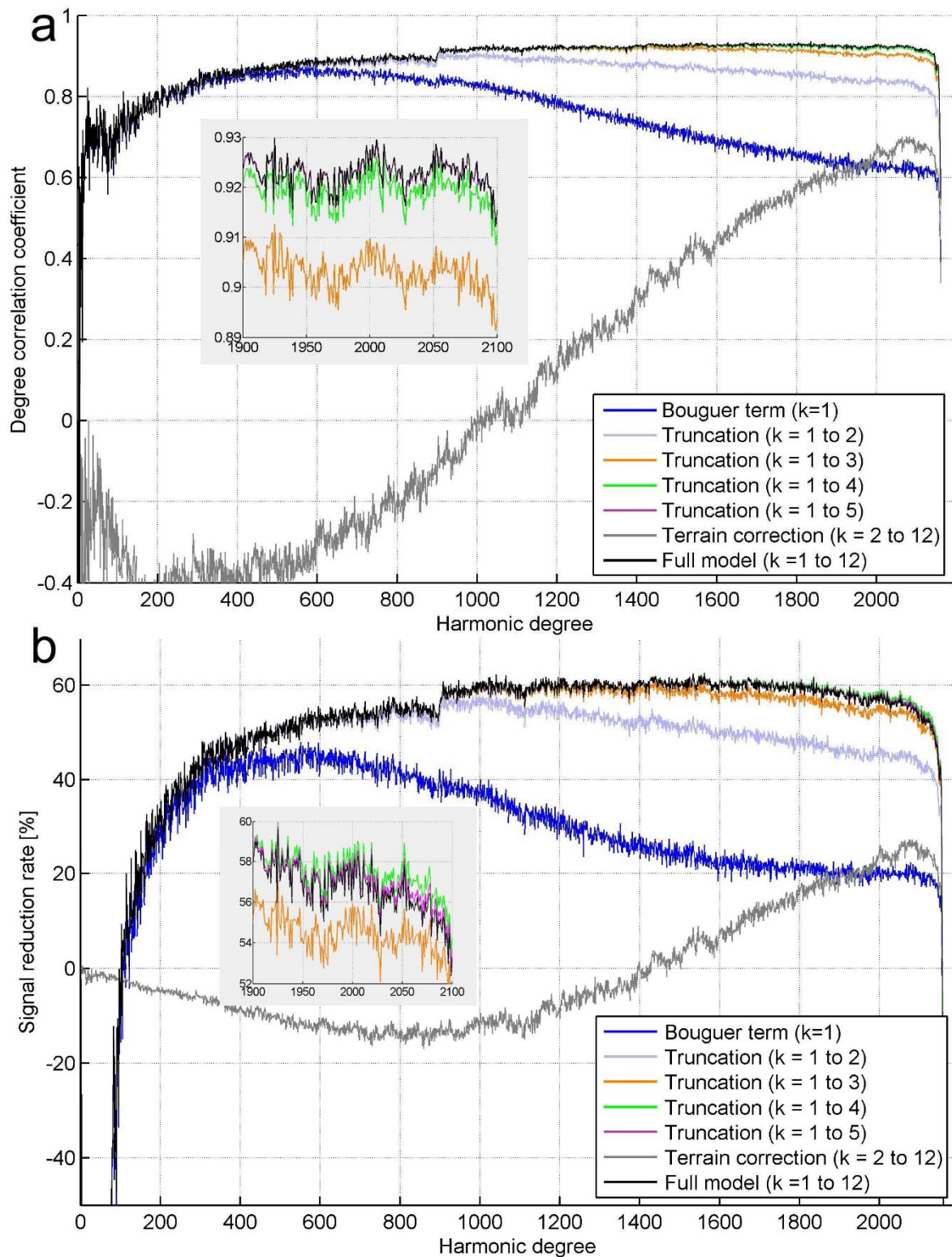
Fig. 7. Approximation effects associated with spectral forward modelling, Top: Effects on CCs, Bottom: effects on RRs. The spherical model sphEGM2008 is compared with the topographic potential model dV_SPH_Earth2014 (k= 1 to 12) and truncations thereof. Case k=1 correlates sphEGM2008 and a spherical Bouguer plate (blue), case k = 2 to 12 sphEGM2008 and the spherical terrain correction (grey). Indicators are also shown between sphEGM2008 and various dV_SPH_Earth2014 truncations (e.g., orange for dV_SPH_RET2014 where the contributions of the topography higher than third-power are neglected).

5.6 Different models
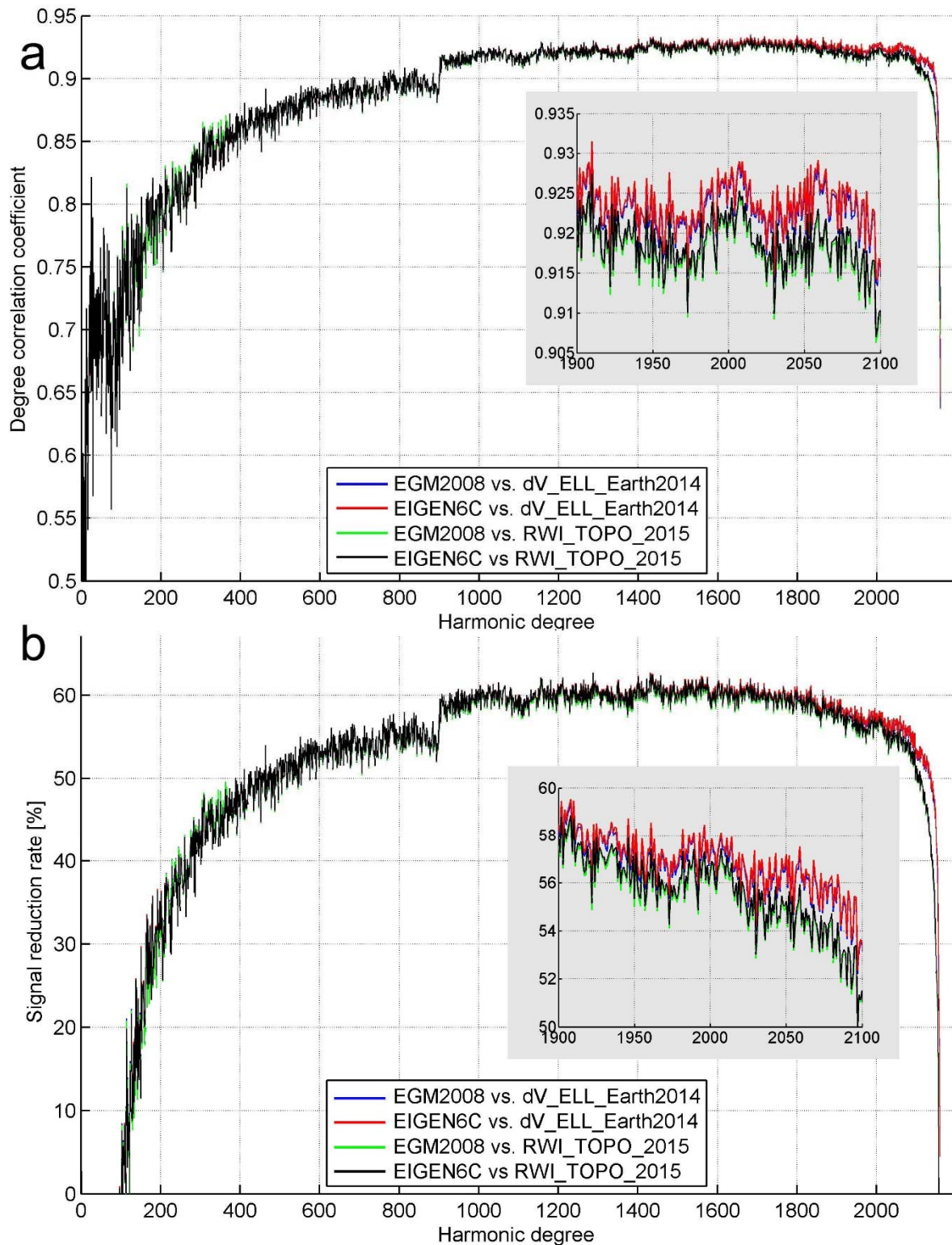
Fig. 8. Effect of the choice of the gravitational potential model (EGM2008 or EIGEN-6C4) and the choice of the topographic potential model (dV_ELL_Earth2014 or RWI_TOPO_2015) on the correlation measures. Top: correlation coefficients, Bottom: signal reduction rates. All models shown were transformed from SHCs to EHCs, which is consistent with the underlying ellipsoidal approximation level.

To justify the choice of the gravitational and topographical potential models used in this study, CCs and RRs are shown in Fig. 8 for two models representing the gravitational potential (EGM2008 and EIGEN-6C4), and two models representing the topographic potential (dV_ELL_Earth2014 and RWI_TOPO_2015), also see Table 2. Different to EGM2008, EIGEN-6C4 uses GOCE gravity data to harmonic degrees of ~300, updated GRACE data to define the long wavelengths, and newer marine gravity data over the oceans, while synthesized EGM2008 is used over land areas to define the short scales (Förste et al. 2015). The two topographic potential models dV_ELL_Earth2014 and RWI_TOPO_2015 are the most-up-to-date "models relating to topography" of ICGEM. Both are based on the same global topography model (Earth2014), but rely on different processing techniques (see Sect. 4.2).

All models have in common a spectral resolution of degree-2190, ellipsoidal approximation, and represent the potential in terms of SHCs. To avoid biases in the CCs and RRs, the SHCs of all four models – as available from ICGEM – were transformed to EHCs (Sect. 2.3), and CCs and RRs were computed from the EHCs. From Fig. 8, CCs and RRs are very close together among all four possible combinations of gravitational and topographic potential models over most of the spectrum. Neither the CCs nor RRs are capable of sensing benefits related to the use of improved satellite data (GRACE and GOCE), as used in EIGEN-6C4, in a global sense. Note that with localisation, the benefits conferred by the GOCE-mission can be well sensed, cf. Hirt et al. (2012, 2015).

At short spatial scales, say around degree ~1900 and higher, both the CCs and RRs indicate some, albeit small, differences between the four model combinations. In any combination, RRs are about ~0.2%-point larger, when the EIGEN-6C4 model is used instead of EGM2008. This might suggest that the resolution of marine gravity, as used in EIGEN-6C4, has improved over that used in EGM2008.

From a cross-comparison between the two topographic potential models dV_ELL_Earth2014 and RWI_TOPO_2015, RRs are consistently about 1%-2%-point larger for dV_ELL_Earth2014 in the band of degrees 1900 to 2100, and this value increases to ~10% near degree 2150. As such, the dV_ELL_Earth2014 topographic potential model offers a slightly better agreement with the gravitational potential models, and this serves as another check on the spectral forward-modelling techniques applied in Sect 3.1.

Altogether, the comparisons in Fig. 8 show that the choice of topographic potential model or gravitational potential model has rather minor impact on the resulting CC and RR curves.

6 Discussion of results in the context of the literature

In this section, some related results on the relation between the topographic and gravitational potential that can be found in the contemporary literature shall be discussed in the context of the previous sections. We restrict this discussion on global correlation studies using EGM2008 as model representing the gravitational potential to 5 arc-min resolution. Degree correlation coefficients between topographic potential models and EGM2008 were published, e.g., in Novak (2010), Claessens and Hirt (2013), Wieczorek (2015), Grombein et al. (2016) and Rexer et al. (2016).

Novak (2010) used the DTM2006.0 (Pavlis et al. 2007) topography/bathymetry model to represent the topographic masses of land topography, ocean bathymetry and atmosphere. A mass-layer approach based on spherical approximation (Sect. 2.3) and third-order expansions (Sect. 3.1) was applied to forward-model the topographic potential. Novak (2010) obtained correlation coefficients of about +0.7 (at degree 1800) and +0.6 (at degree 2100) between the potential implied by land topography and EGM2008 (Fig. 2 ibid), and attributes the "*lack of larger correlation*" to "*deeper mass anomalies and isostatic compensation inside the solid Earth that are reflected by EGM08*" (Novak 2010, p20).

However, with the results presented in our paper (Fig. 1 and especially Fig. 6) we conclude that the lack of larger correlation is solely the result of comparing models with different approximation levels (SA for the topographic potential, and EA for gravitational potential). Not shown here, but we have cross-compared the dV_SPH_LAND2014 (SA) model with EGM2008 (EA) and were able to reproduce the correlation curve published in Novak (2010, Fig 2). From our Fig. 7, when identical approximation levels are used for both models compared, CCs consistently exceed +0.9 in spectral band of degrees 1800 to 2100. This demonstrates substantial short-scale correlation between EGM2008 and the potential of the land topographic masses. As an aside, the truncation of the series expansion to third-order in Novak et al. (2010) has only a minor impact on the CCs at short scales (at the level of ~0.02), cf. Fig. 7.

Degree CCs or RRs very similar to those shown by the green curve in Fig. 1 were published in Claessens and Hirt (2013, Fig. 11 ibid), Wieczorek (2015, Fig. 2), Grombein et al. (2015, Fig. 16) and Rexer et al. (2016, Fig. 10). The cited works have in common that the underlying topographic potential models are represented in terms of SHCs and based on EA. An exception is the forward modelling done in Wieczorek (2015), where an Earth shape model (representation of surface relief in terms of geocentric radii) is referred to a reference sphere; the resulting topographic potential model behaves like the models based on EA, as far as the CCs with EGM2008 are concerned.

In all of these cited works, the CC or RR curves show a maximum agreement between topographic and gravitational potential near degree ~1000, with steadily declining correlation towards degree 2190. Little discussion is included in the cited references on the declining CCs beyond degree 1000, apart from Rexer et al. (2016), who state: "*However, the degree correlation computed from the (original) spherical harmonic models reaches a maximum correlation of 0.93 near degree ~1000, after which the correlations decrease again (and stay above 0.8). This is against all expectations, since the short-scale signals of the gravity field are driven by the topographic masses. Hence, an increase in the correlation is to be expected. The reason for this behaviour is that spherical harmonic models in ellipsoidal approximation (like EGM2008 and most other models found at ICGEM) cannot be used in small bands (band limited) because of dependencies among the coefficients that affect the ellipsoidal approximation.*"

With the results presented in our study (Fig. 4 and Appendix A2), it can be confidently concluded that the previously published CC-curves overestimate the correlation at medium harmonic degrees (say from 200 to 1200), while underestimating it at high harmonic degrees (say from degree 1500 to 2190). More realistic CCs are obtained in comparisons between topographic and gravitational potential models when both models are based on EA and EHCs, or SA and SHCs (Sect. 5.1). In these cases, the CCs show increasing or constant correlation at high degrees. However, even when the models are compatible (e.g., SA and SHCs), the reduction rates do not increase beyond degree ~1500, which we attribute to the marine/bathymetric gravity fields not reaching full resolution to 5 arc-min scales (cf. Sect. 5.4).

7 Recommendations and conclusions

This paper has investigated a number of approximation effects that can be relevant in comparisons between high-degree models of the topographic and gravitational potential. Some of the effects investigated have a rather subtle influence, while others have quite a substantial impact on correlation studies when high-degree geopotential models such as EGM2008 are involved. Our study has shown the importance that both models be as "compatible" as possible.

First, when the topographic and gravitational potential models are based on different approximation levels (e.g., one model based on spherical approximation and the other on ellipsoidal

approximation), the short-scale agreement is strongly underestimated, e.g., a correlation of +0.58 instead of +0.92 is obtained at degree 2100. It is therefore important to ensure identical levels of approximation in both models.

Second, even when both models are based on the same level of approximation, the degree correlations and reduction rates are biased over most of the spectrum if the models are represented in SHCs while relying on ellipsoidal approximation. This is the case, e.g., for ICGEM gravity models. The bias reaches amplitudes of about 0.05 (in terms of degree correlation) or 10%-points (in terms of reduction rates). Two ways to avoid the bias were shown in this paper, namely either comparing models 1) represented as EHCs and relying on ellipsoidal approximation or 2) represented in terms of SHCs and relying on spherical approximation. The necessary transformations are described in Sect. 2 and 3 of this paper.

Further, it is recommended to use topographic potential models based on 3D mass-layer modelling. The latter avoids approximation errors associated with RET mass compression, and ensures better short-scale agreement with the gravitational potential. The associated gain in correlation is about 0.01 (in terms of CC) or ~4%-points (in terms of reduction rates) at short scales.

With the insights gained in this work, more realistic (in the sense of unbiased) values for correlation measures are obtained in comparisons between gravitational and topographic potential models (or constituents thereof, e.g., potential of land topography or water masses). This can be useful for future correlation studies or quality assessments of new high-degree geopotential or topographic potential models.

Acknowledgements

Appendix

A1 Properties of the sphEGM2008 model

The transformation described in Sect. 3.2 was applied to obtain the spherical transform of EGM2008, named sphEGM2008 in this paper. The sphEGM2008 model represents Earth's geopotential as if the field-generating masses were arranged relative to a sphere, and not relative to an ellipsoid (which is the case for EGM2008). As the main benefit of such a "spherical" high-degree spectral model of the geopotential, it can be readily and meaningfully applied in band-limited operations, such as degree-wise syntheses or correlation coefficient computations. This is fundamentally different from EGM2008 (or any other high-degree model of the geopotential represented as SHCs and relying on ellipsoidal approximation) where its SHCs can only be used within the full band-width (i.e., band of degrees from 2 to 2190).

Because the sphEGM2008 approach is not yet well known in the gravity field community, some exemplary results shall illustrate the differences between the SHC model representations of sphEGM2008 (this work) and EGM2008 (Pavlis et al. 2012). In all gravity syntheses presented next,

- the sphEGM2008 model coefficients are evaluated at some height above the reference sphere (sphere with radius of 6,378,137.0 m), and

- the EGM2008 model coefficients are evaluated at the same height above the reference ellipsoid (ellipsoid with semi-major axis of 6,378,137.0 m, and semi-minor axis of 6,356,752.3141 m, taken from the GRS80 parameters),

such that choice of reference surfaces and evaluation points is mutually consistent.

Figure 9a shows global gravity disturbances from the sphEGM2008 model, evaluated at 9,000 m height above the reference sphere in the full band-width of the model (degrees 2 to 2240). These are in very close agreement with gravity disturbances of the EGM2008 model (evaluated at 9,000 m height above the reference ellipsoid in the full band-width of degrees 2 to 2190, as is seen in Fig. 9b. The differences between the full-banded evaluations of sphEGM2008 and EGM2008 (Fig. 9b) can be interpreted as a spherical effect, reflecting the non-identical mass arrangement in spherical approximation (sphEGM2008) and ellipsoidal approximation (EGM2008).

The differences show a North-South structure and correlate spatially with North-South-aligned gravity structures (compare Figs. 9a and 9b). They are small (min/max/rms = -0.64/+0.77/0.07 mGal) at 9,000 m above the reference spheres, and would somewhat increase if the syntheses were done at the respective reference surfaces (min/max/rms = -1.28/+1.82/0.09 mGal). A reduction of the differences (e.g., through modelling and correction of the spherical effect in the spectral domain) was not attempted in this work.

We note that the sphEGM2008 model features additional signals at harmonic degrees larger than 2160, which are a consequence of the windowing effect in the transformation (Eq.13). The sphEGM2008 signal strength associated in band of degrees 2161-2190 does not exceed 0.09 mGal anywhere on the globe (at 9,000 m height), which is almost one order of magnitude smaller than the spherical effect. Beyond degree 2190, the signal strength is always smaller than 5×10^{-5} mGal. All in all, the additional coefficients beyond degree 2160 can be considered to be of minor relevance in practical applications of sphEGM2008.

Figures 10 and 11 illustrate the benefits of a spherically approximated geopotential model (sphEGM2008) over an ellipsoidally approximated geopotential model (EGM2008). For the North Pole region, Fig. 10 shows gravity disturbances from both models, truncated at harmonic degree 2000. The sphEGM2008 model is seen to be free of truncation effects, while these are very clearly manifested as striations for EGM2008. We emphasize that the striations of course disappear when EGM2008 is evaluated in its full band-width.

Figure 11 compares band-limited gravity disturbances from sphEGM2008 and EGM2008 in harmonic degrees of 1001-2000 (spatial scales of 5.4 to 10.8 arc-min). The striations visible in Fig. 11 render any band-limited application of EGM2008 (or any other high-degree model) near the poles and in short-scale bands impossible. In contrast, sphEGM2008 is not subjected to striations (also see Sect. 3.2), so can be used in a band-limited fashion (narrow bands or degree-wise), e.g., in syntheses or correlation coefficient computations as in this paper. As a drawback of band-limited applications of sphEGM2008 model, a part of the gravity signals associated with the spherical effect (Fig. 9 bottom) are neglected. This drawback can be overcome by using the EHCs of EGM2008 in band-limited ellipsoidal harmonic syntheses, which however, was not performed in this study.

A2 The bias in degree correlation coefficients and reduction rates

To obtain insight into the reason behind the biased CC and RR values (cf. Sect 5.2), we have investigated gravity effects in the space domain. The four models EGM2008, sphEGM2008, dV_ELL_Earth2014 and dV_SPH_Earth2014 were used to synthesise gravity disturbances implied by single spherical harmonic degrees. The syntheses were done at the surface of the reference sphere

(sphEGM2008 and dV_SPH_Earth2014) and reference ellipsoid (EGM2008 and dV_ELL_Earth2014) in terms of 5 arc-min global grids equally spaced in geocentric latitude. As harmonic degree of evaluation, we have chosen degree 500 where large differences in CCs and RRs were observed (Sect. 5.2). CCs and RRs were computed as described in Hirt (2014). Figure 12 shows the computed gravity disturbances over Northern Europe. Note that dV_ELL_Earth2014 and EGM2008 were evaluated at the reference ellipsoid, while dV_SPH_Earth2014 and sphEGM2008 were evaluated at the reference sphere.

Among the gravitational and topographic potential models that rely on EA, a regional correlation of +0.89 and reduction rate of 54.1 % is observed (Fig. 12a, 12b).

- This is larger than the corresponding values obtained among the gravitational and topographic potential models that are based on SA (CC of +0.85 and RR of 47.1%), cf. Fig. 12c, 12d.
- The differences between EGM2008 and sphEGM2008 (Fig. 12e) represent in approximation the windowing effect contained in the gravitational potential model EGM2008 (caused by Eq. 6). Accordingly, the differences dV_ELL_Earth2014 minus dV_SPH_Earth2014 (Fig. 12f) reveal the windowing effect contained in the topographic potential model dV_ELL_Earth2014 (caused by Eq. 9).
- Figures 12e, 12f shows that the windowing effect produces "striations" that are strongly correlated (in our example +0.90 and RR of 55.4%). Note that the striations tend to increase with degree and equatorial distance.
- The gravity disturbances shown in Fig. 12 (top row) are the sum of those shown in the middle row (gravity signals in spherical approximation) and bottom row (striations).
- Thus, it is the high correlation between the striations (bottom row) that drives up the correlation between the ellipsoidal model pairs (top row), compared to the spherical model pairs (middle row).

It becomes obvious that the striations produce apparent correlation, which is non-existent in the actual gravity signals implied by harmonic degree 500 (Fig. 12, middle row). Strictly speaking, the windowing effect (Eq. 6 and 9) introduces functional (aka geometric) correlations among the coefficients of the models based on ellipsoidal approximation, which lead to higher degree correlations than in spherical approximation.

From a global comparison instead of a regional comparison (as in Fig. 12), very similar results can be obtained. Globally, between the ellipsoidal gravitational and topographic potential models, a CC of +0.90 and RR of 57.0% is obtained. In SA, the correlation measures are lower (CC of +0.86 and RR of 48.9 %). When the windowing effect is isolated in approximation (as in Fig. 12, bottom row, but here globally), a CC of +0.91 and RR of 58.1 % is obtained among the two fields. These values, which are in good agreement with those obtained directly from the harmonic coefficients in Sect. 5, demonstrate that correlation measures computed in ellipsoidal approximation may be biased.

The described experiment can be repeated for all other harmonic degrees. For high degrees, e.g., degree 2000, the effect reverses, in that, a lower correlation between the gravitational and topographic potential striations biases the correlations towards values too low in case of ellipsoidal approximation: For degree 2000, SA yields a CC of +0.92 and RR of 55.2 % (vs. CC of +0.86 and 47.6 % in EA). For the windowing effect (as in Fig. 12 bottom row, but globally and degree 2000), a CC of +0.86 and RR of 47.6% is obtained, which is largely responsible for the values observed in EA.

Finally, it is emphasised that the striations shown in Figs. 10 to 12 are not to be interpreted as model errors. They are vitally important constituents of the SHCs needed to correctly represent the EGM2008 gravity signals over the complete full band-width (degrees 2 to 2190) when a potential

model is based on ellipsoidal approximation. As shown above, the windowing effect only ever matters if the SHCs of an ellipsoidally approximated model is used in a band-limited manner at high degrees, though it shouldn't.
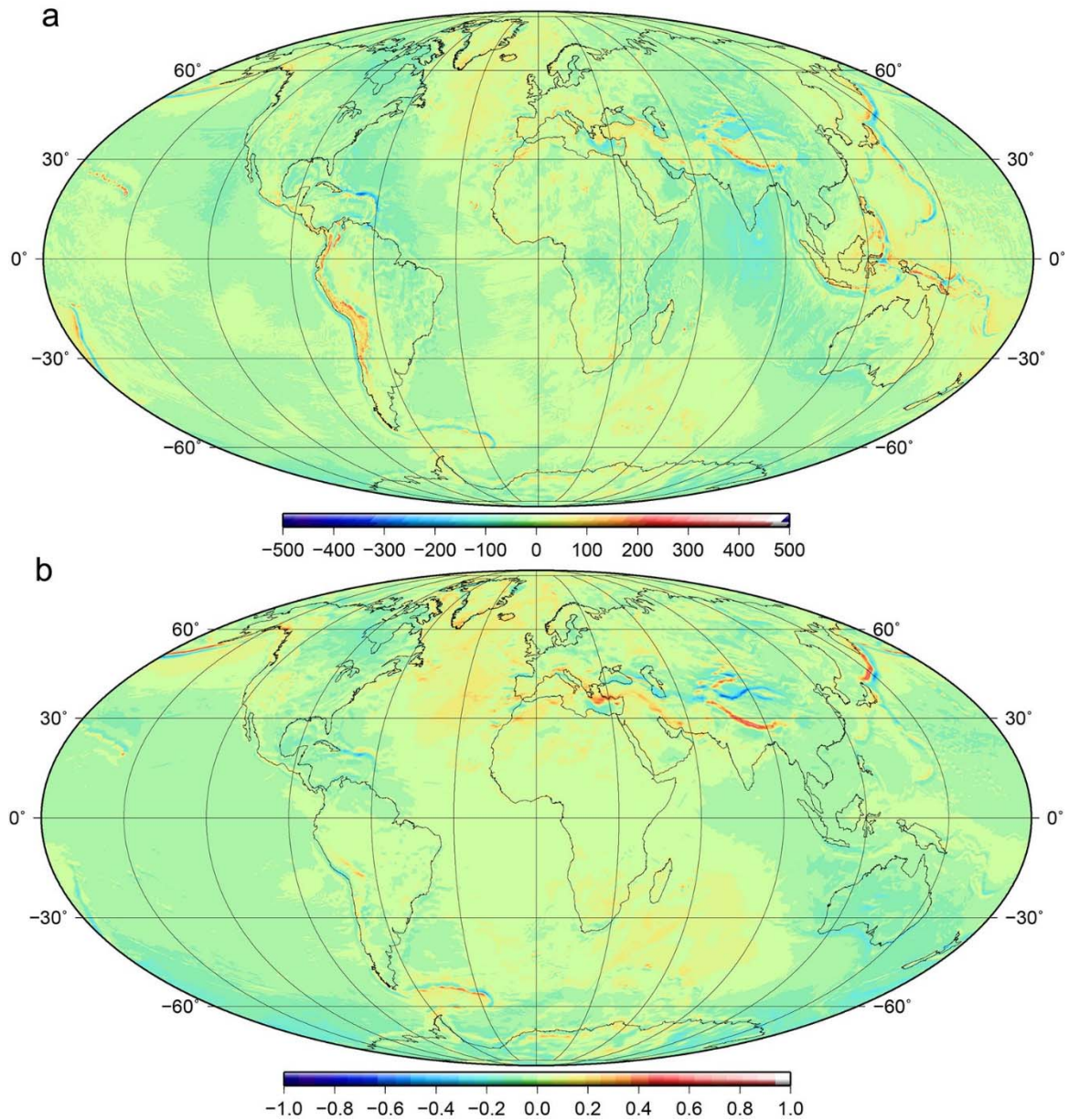

Fig. 9. Top: Gravity disturbances from the sphEGM2008 model, synthesized in band 2 to 2240 at a constant height of 9000 m height above the reference sphere. Bottom: Spherical effect = discrepancies between the models EGM2008 (synthesized in band 2 to 2190 at 9000 m height above reference ellipsoid and sphEGM2008 (synthesized in band 2 to 2240 at 9000 m height above the reference sphere). Units in mGal, grids equally spaced in terms of geocentric latitudes. The figure illustrates that the differences (reflecting the effect of the different mass arrangement in ellipsoidal and spherical approximation) are rather small compared to the sphEGM2008 gravity signal (top).
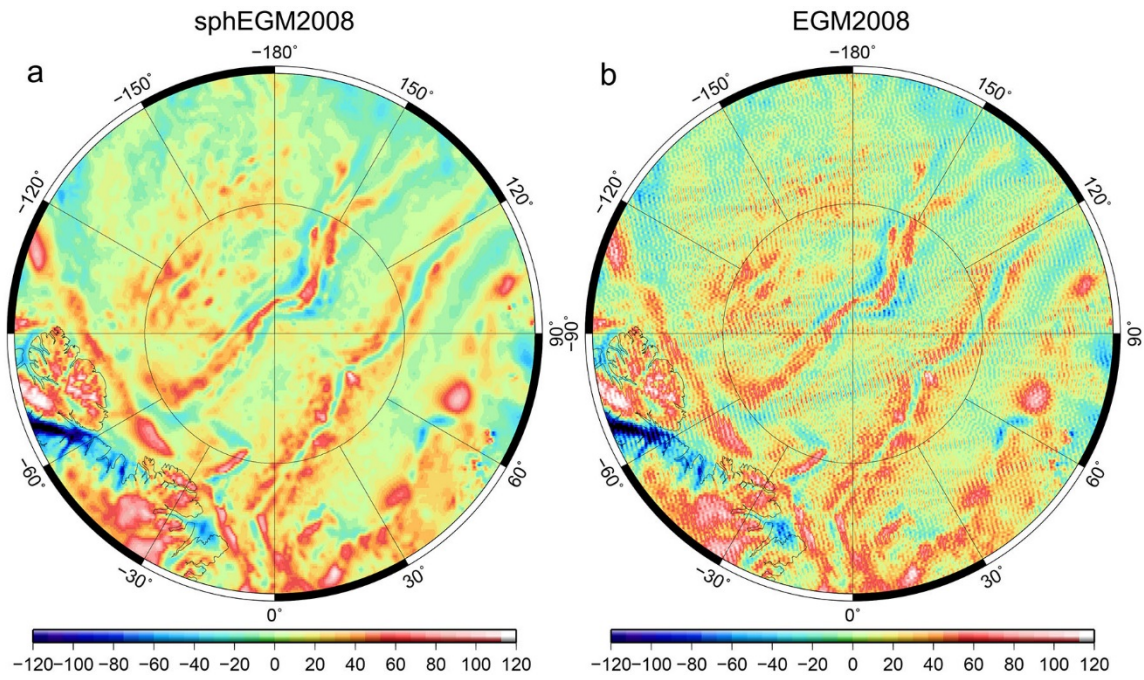
Fig. 10. Gravity disturbances synthesized in band 2 to 2000 at 4000 m height above reference. Left: sphEGM2008 model, reference surface = sphere, Right: EGM2008, reference surface = GRS80 ellipsoid. Units in mGal; grids equally spaced in terms of geocentric latitude; area shown is Northern Polar region (80°-90° geocentric latitude). The figure illustrates that band-limited operations such as truncation below the maximum model degree are permitted for sphEGM2008, while high-latitude striations prohibit the band-limited use of EGM2008 (as SHC representation).
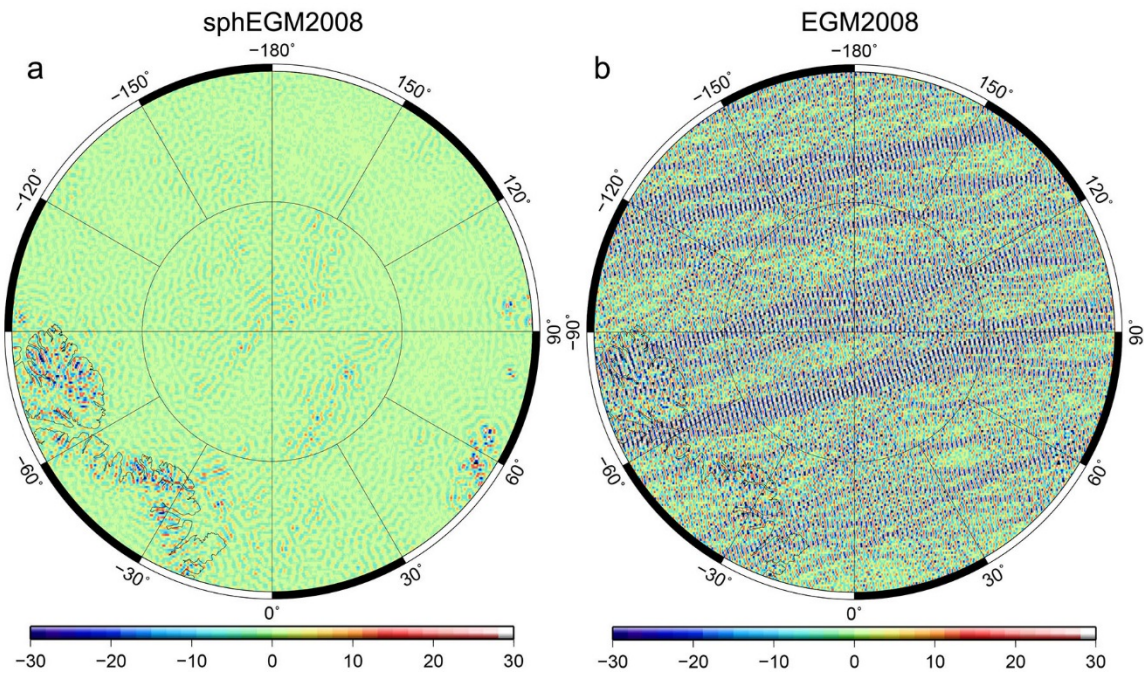

Fig. 11. Gravity disturbances synthesized in band 1001 to 2000 at 4000 m height above reference. Left: sphEGM2008 model, reference surface = sphere, Right: EGM2008, reference surface = GRS80 ellipsoid. Units in mGal. The figure illustrates that band-limited operations such as evaluations of high degree bands are permitted for sphEGM2008, while high-latitude striations prohibit the band-limited use of EGM2008 (as SHC representation).
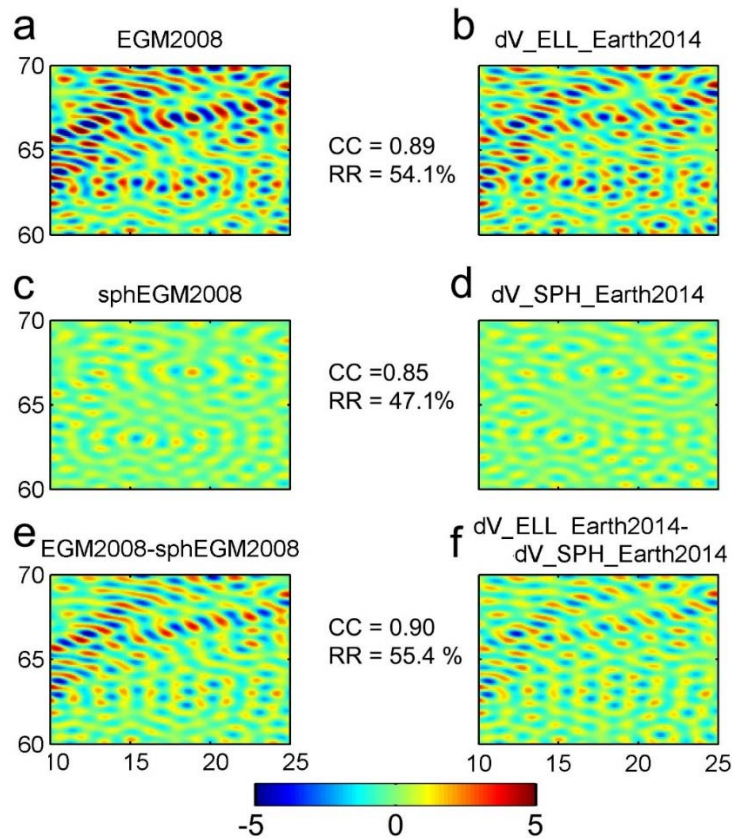
Fig. 12. Gravity disturbances implied by harmonic degree 500 over Northern Europe (10° to 25° longitude, 60° to 70° geocentric latitude), obtained from six models or combinations. Top row: EGM2008 and dV_ELL_Earth2014 (both based on ellipsoidal approximation), middle row: sphEGM2008 and dV_SPH_Earth2014 (both based on spherical approximation), bottom row: differences EGM2008-sphEGM2008 and dV_ELL_Earth2014-dV_SPH_Earth2014). The figure shows that the striations (bottom row) produce a bias that is the reason for the higher correlation between the ellipsoidal pairs (top row) compared to the more realistic values for the spherical pairs (middle row).

References

Ananda, MP, Sjogren WL, Phillips RJ Wimberly RN, Bills BG (1980) A low-order global gravity field of Venus and dynamical implications. J Geophys Res 85:8303–8318. doi: 10.1029/JA085iA13p08303

Andersen OB (2010) The DTU10 Global Gravity field and mean sea surface –improvements in the Arctic Presented at the 2nd Gravity Field Symposium of IAG in Fairbanks, Alaska

Andersen OB, Knudsen P, Berry PAM (2010) The DNSC08GRA global marine gravity field from double retracked satellite altimetry. J Geod 84(3):191–199. doi: 10.1007/s00190-009-0355-9

Balmino G, Vales N, Bonvalot S, Briais A (2012) Spherical harmonic modelling to ultra-high degree of Bouguer and isostatic anomalies. J Geod 86(7):499–520. doi:10.1007/s00190-011-0533-4

Bamber JL, Griggs, JA, Hurkmans RT et al. (2013) A new bed elevation dataset for Greenland. The Cryosphere 7:499–510

Becker JJ, Sandwell, DT, Smith, WHF et al. (2009) Global Bathymetry and Elevation Data at 30 Arc Seconds Resolution: SRTM30_PLUS. Marine Geod 32(4):355-371. doi:10.1080/01490410903297766

Blakeley RJ (1996), Potential Theory in Gravity and Magnetic Applications. Cambridge: Cambridge University Press.

Chambat, F, Valette B (2005) Earth gravity up to second order in topography and density, Physics Earth Plan Int 151(1-2):89-106. doi:10.1016/j.pepi.2005.01.002

Claessens, SJ (2005) New relations among associated Legendre functions and spherical harmonics. J. Geod 79(6-7):398-406. doi: 10.1007/s00190-005-0483-9

Claessens, SJ (2006) Solutions to Ellipsoidal Boundary Value Problems for Gravity Field Modelling, PhD thesis, Curtin University of Technology, Department of Spatial Sciences, Perth, Australia.

Claessens SJ, Featherstone WE (2008) The Meissl scheme for the geodetic ellipsoid. J Geod 82(8):513–522. doi:10.1007/s00190-007-0200-y

Claessens SJ, Hirt C (2013) Ellipsoidal topographic potential: new solutions for spectral forward gravity modeling of topography with respect to a reference ellipsoid. J Geophys Res 118(11):5991–6002. doi:10.1002/2013JB010457

Claessens, SJ (2016) Spherical harmonic analysis of a harmonic function given on a spheroid. Geophys. J Int 206(1):142-151. doi:10.1093/gji/ggw126

Colombo O (1981) Numerical methods for harmonic analysis on the sphere. Tech. Rep. Rep. No. 310, The Ohio State University

Forsberg R, Tscherning CC (1981) The use of height data in gravity field approximation by collocation. J Geophys Res 86(B9)7843-7854.

Förste C, Bruinsma SL., Abrikosov O et al. (2015), EIGEN-6C4 The latest combined global gravity field model including GOCE data up to degree and order 2190 of GFZ Potsdam and GRGS Toulouse. doi:10.5880/icgem.2015.1.

Fretwell P, Pritchard HD, Vaughan DG, et al. (2013) Bedmap2: improved ice bed, surface and thickness datasets for Antarctica. The Cryosphere 7:375-393.

Grombein, T, Seitz K, Heck B (2016) The Rock–Water–Ice Topographic Gravity Field Model RWI_TOPO_2015 and Its Comparison to a Conventional Rock-Equivalent Version. Surv Geophys 37(5):937-976. doi:10.1007/s10712-016-9376-0.

Heiskanen WA, Moritz H (1967) Physical Geodesy. San Francisco: WH Freeman.

Hirt C, Reußner E, Rexer M, Kuhn M (2016) Topographic gravity modelling for global Bouguer maps to degree 2,160: Validation of spectral and spatial domain forward modelling techniques at the 10 microgal level, J Geophys Res – Solid Earth 121(9),6846–6862. doi:10.1002/2016JB013249

Hirt C, Rexer, M (2015) Earth2014: 1 arc-min shape, topography, bedrock and ice-sheet models - available as gridded data and degree-10,800 spherical harmonics. Int J Appl Earth Obs Geoinf 39, 103-112, doi:10.1016/j.jag.2015.03.001

Hirt C (2014) GOCE's view below the ice of Antarctica: Satellite gravimetry confirms improvements in Bedmap2 bedrock knowledge. Geophys Res Lett 41(14), 5021- 5028. doi: 10.1002/2014GL060636.

Hirt C, Kuhn M (2014) A band-limited topographic mass distribution generates a full-spectrum gravity field – gravity forward modelling in the spectral and spatial domain revisited. J Geophys Res– Solid Earth 119(4):3646–3661. doi: 10.1002/2013JB010900

Hirt C, Kuhn M, Featherstone WE, Göttl, F (2012) Topographic/isostatic evaluation of new-generation GOCE gravity field models. J Geophys Res – Solid Earth 117:B05407. doi:10.1029/2011JB008878

Hirt C, Kuhn M (2012) Evaluation of high-degree series expansions of the topographic potential to higher-order powers. J Geophys Res – Solid Earth 117:B12407. doi:10.1029/2012JB009492

Hirt C, Rexer M, Claessens SJ (2015) Topographic evaluation of fifth-generation GOCE gravity field models – globally and regionally. Newton's Bulletin. 5:163-186.

Hobson EW (1965) The theory of spherical and ellipsoidal harmonics. Chelsea Publishing Company, New York, 500 pp.

Holmes SA, Pavlis NK (2007) Some aspects of harmonic analysis of data gridded on the ellipsoid, in Gravity Field of the Earth, Proceed. 1st International Symposium of the International Gravity Field Service, Istanbul, Turkey, J. Harita Dergisi, 73(18), 151–156, (General Command of Mapping), Ankara, Turkey.

Hu X, Jekeli, C (2015) A numerical comparison of spherical, spheroidal and ellipsoidal harmonic gravitational field models for small non-spherical bodies: examples for the Martian moons. J Geod 89(2):159–177. doi: 10.1007/s00190-014-0769-x

Jarvis A, Reuter HI, Nelson A, Guevara E (2008) Hole-filled SRTM for the globe v4.1, Available from the CGIAR-SXI SRTM 90m database at: http://srtm.csi.cgiar.org.

Jekeli C. (1988) The exact transformation between ellipsoidal and spherical harmonic expansions, Manuscr Geod 13:106–113.

Kaula WM (1992), Properties of the Gravity Fields of Terrestrial Planets. In: From Gravity to Greenland: Charting Gravity with Space and Airborne instruments, Proc of Symposium 110 (ed. O. Colombo), Springer, New York, Berlin, Heidelberg

Konopliv AS , Banerdt WB, Sjogren WL (1999) Venus Gravity: 180th Degree and Order Model. Icarus 139, 3–18.

Konopliv AS, Park RS, Yuan D-N et al (2013) The JPL lunar gravity field to spherical harmonic degree 660 from the GRAIL Primary Mission. J Geophys Res - Planets 118(7), 1415-1434, doi:10.1002/jgre.20097

Konopliv AS, Park RS, Folkner WM (2016) An improved JPL Mars gravity field and orientation from Mars orbiter and lander tracking data. Icarus 274:253-260. doi:10.1016/j.icarus.2016.02.052

Kuhn M, Featherstone, WE, Kirby JF (2009) Complete spherical Bouguer gravity anomalies over Australia. Australian J. Earth Sci 56(2):213-223. doi:10.1080/08120090802547041

Kuhn M, Hirt C (2016) Topographic gravitational potential up to second-order derivatives: an examination of approximation errors caused by rock-equivalent topography (RET). J Geod 90(9):883-902. doi:10.1007/s00190-016-0917-6

Lambeck K (1976) Lateral density anomalies in the upper mantle. J Geophys Res 81(35):6333–6340. doi:10.1029/JB081i035p06333

Lee WHK, Kaula WM (1967) A spherical harmonic analysis of the Earth's Topography. J Geophys Res 72(2):753-758. doi:10.1029/JZ072i002p00753

Lemoine FG, Goossens S, Sabaka TJ, et al. (2014) GRGM900C: A degree-900 lunar gravity model from GRAIL primary and extended mission data. Geophys Res Lett 41(10): 3382–3389. doi: 10.1002/2014GL060027

Lowes FJ, Winch DE (2012), Orthogonality of harmonic potentials and fields in spheroidal and ellipsoidal coordinates: application to geomagnetism and geodesy. Geophys J Int 191:491–507. doi: 10.1111/j.1365-246X.2012.05590.x

Mazarico E, Lemoine FG, Han SC, Smith DE (2010) GLGM-3: a degree-150 lunar gravity model from the historical tracking data of NASA Moon orbiters J Geophys Res 115:E05001. doi:10.1029/2009JE003472

McGovern, PJ, Solomon SC, Smith DF et al. (2002) Localized gravity/topography admittance and correlation spectra on Mars: implications, for regional and global evolution. J Geophys Res 107(12):5136. doi:10.1029/2002JE001854, 2002.

Novák P (2010) High Resolution Constituents of the Earth's Gravitational Field. Surv Geophys 31:1. doi:10.1007/s10712-009-9077-z

Pavlis N, Factor J, Holmes S (2007) Terrain-related gravimetric quantities computed for the next EGM. In: Dergisi H (ed) Proceedings of the 1st international symposium of the international gravity field service, vol 18, pp 318–323

Pavlis N, Holmes S, Kenyon S, Factor J (2012) The development and evaluation of the Earth Gravitational Model 2008 (EGM2008). J Geophys Res – Solid Earth 117:B04406. doi:10.1029/2011JB008916

Pavlis N, Holmes S, Kenyon S, Factor J (2013) Correction to the development and evaluation of the Earth Gravitational Model 2008 (EGM2008). J Geophys Res – Solid Earth 118(5): 2633-2633. doi: 10.1002/jgrb.50167

Phillips RJ, Lambeck K (1980) Gravity Fields of the Terrestrial Planets: Long-Wavelength Anomalies and Tectonics. Rev Geophys Space Phys 18(1):27-76. doi:10.1029/RG018i001p00027

Rapp RH (1982) Degree variances of the Earth's potential, topography and its isostatic compensation. Bull Geod 56:84-94, doi:10.1007/BF02525594

Rexer M, Hirt C (2015), Spectral analysis of the Earth's topographic potential via 2D-DFT -a new data-based degree variance model to degree 90,000. J Geod 89(9):887-909. doi: 10.1007/s00190-015-0822-4

Rexer M, Hirt C, Claessens SJ, Tenzer R (2016) Layer-based modelling of the Earth's gravitational potential up to 10km-scale in spherical harmonics in spherical and ellipsoidal approximation. Surv Geophys 37(6):1035-1074. doi:10.1007/s10712-016-9382-2

Rummel R, Rapp R, Sünkel H, Tscherning C (1988) Comparisons of global topographic/isostatic models to the Earth's observed gravity field. OSU report 388, Ohio State University

Sandwell DT, Smith WHF (2009) Global marine gravity from retracked Geosat and ERS-1 altimetry: Ridge Segmentation versus spreading rate. J Geophys Res 114:B01411. doi:10.1029/2008JB006008

Sanso F, Sideris M (2013) Geoid Determination - Lecture Notes in Earth Sciences, vol 110, Springer-Verlag Berlin, Heidelberg, chap Harmonic Calculus and Global Gravity Models

Sebera J, Bouman J, Bosch W (2012), On computing ellipsoidal harmonics using Jekeli's renormalization, J Geod 86(9):713–726. doi:10.1007/s00190-012-0549-4

Simons M., Solomon SC, Hager BH (1997), Localization of gravity and topography: conestraints on the tectonics and mantle dynamics of Venus. Geophys J Int 131:24-44. doi:10.1111/j.1365-246X.1997.tb00593.x

Torge W, Müller J (2012) Geodesy. 4th Edition. Berlin, New York: W. de Gruyter.

Tenzer R., Chen W, Tsoulis D, et al (2015) Analysis of the Refined CRUST1.0 Crustal Model and its Gravity Field. Surv Geophys 36(1):139-165. doi:10.1007/s10712-014-9299-6

Tenzer R, Abdalla A, Vajda P, Hamayun (2010) The spherical harmonic representation of the gravitational field quantities generated by the ice density contrast. Contrib Geophys Geod 40(3):207–223. doi:10.2478/v10126-010-0009-1

Torge W, Müller J (2012) Geodesy. 4th Edition. Berlin, New York: W. de Gruyter.

Tsoulis D, Patlakis K (2013) A spectral assessment review of current satellite-only and combined Earth gravity models. Rev Geophys 51(2):186–243. doi:10.1002/rog.20012

Tscherning, CC (1985) On the long-wavelength correlation between gravity and topography, in Fifth International Symposium Geodesy and Physics of the Earth", G.D.R. Magdeburg, 23–29 September 1984: Symposium Proceedings, edited by H. Kautzleben, Veröffentlichungen des Zentralinstituts für Physik der Erde, 81(2), 134–142, Akademie der Wissenschaften der DDR, Potsdam.

Tziavos, IN, Sideris MG (2013) Topographic reductions in gravity and geoid modeling, in Lecture Notes in Earth System Sciences, 110:337–400, Springer, Berlin Heidelberg.

Wang, YM, Yang X (2013), On the spherical and spheroidal harmonic expansion of the gravitational potential of topographic masses. J Geod 87(10):909–921. doi:10.1007/s00190-013-0654-z

Watts AB (2011) Isostasy, In: Encyclopedia of Solid Earth Geophysics (Ed. Gupta, H. K.): 647-662, Elsevier.

Wieczorek MA, Simons FJ (2005) Localized spectral analysis on the sphere .Geophys J Int 162(3):655-675. doi: 10.1111/j.1365 246X.2005.02687.x

Wieczorek M (2015) 10.05—Gravity and topography of the terrestrial planets. In: Schubert G (ed) Treatise on geophysics, 2nd edn. Elsevier, Oxford, pp 153–193. doi:10.1016/B978-0-444-53802-4.00169-X

Zuber MT, Smith DE, Watkins MM, Asmar SW, Konopliv AS, Lemoine FG, Melosh HJ, Neumann GA, Phillips RJ, Solomon SC, Wieczorek MA, Williams JG, Goossens SJ, Kruizinga G, Mazarico E, Park RS, Yuan DN (2012) Gravity Field of the Moon from the Gravity Recovery and Interior Laboratory (GRAIL) Mission. Science 339(6120):668-671. doi:10.1126/science.1231507.